A new FE post-processor for probabilistic fatigue assessment in the presence of defects and its application to AM parts

S. Romano, S. Miccoli, S. Beretta

PII: S0142-1123(19)30132-X
DOI: https://doi.org/10.1016/j.ijfatigue.2019.04.008
Reference: JIJF 5070

To appear in: *International Journal of Fatigue*

Revised Date: 4 April 2019
Accepted Date: 6 April 2019

Please cite this article as: Romano, S., Miccoli, S., Beretta, S., A new FE post-processor for probabilistic fatigue assessment in the presence of defects and its application to AM parts, *International Journal of Fatigue* (2019), doi: https://doi.org/10.1016/j.ijfatigue.2019.04.008

A new FE post-processor for probabilistic fatigue assessment in the presence of defects and its application to AM parts

S. Romano[a], S. Miccoli[a], S. Beretta[a,*]

[a] *Politecnico di Milano, Department of Mechanical Engineering, Via La Masa 1, I-20156 Milan, Italy*

Abstract

Despite the disruptive benefits of Additive Manufacturing (AM), the application of this technology for safety-critical structural parts in aerospace is still far from being achieved and standardised. The necessity to comply with very strict reliability requirements is hindering this final step because of the large scatter and low reproducibility always associated with AM, especially in terms of fatigue strength. In this regard, manufacturing defects are the most important and complex issue, but several other sources of variability have an effect as well. The AM community and the main aerospace industries involved are starting to agree that damage-tolerant approaches are necessary and that probabilistic methods are best-suited to obtain reliable but not over-constrained assessments.

To address this issue, the authors have developed Pro-FACE, a fully-probabilistic software that aims to robustly assess the fatigue strength and critical locations of complex components in the presence of defects. This paper presents the underlying concept, its implementation and early validation, and a simple application to a space component. The analytical formulation makes this tool ideal to evaluate very low failure probabilities with limited time and effort, which can provide valuable information to significantly improve part design and qualification.

Keywords: Additive Manufacturing; Fatigue; Defects; Failure Probability

*Corresponding author
Email address: stefano.beretta@polimi.it (S. Beretta)

NOMENCLATURE

a - crack size

h - size defining the surface volume

k_σ - slope of the Wöhler curve

n - number of defects

r - material resistance

r_{eq} - radius of the circle equivalent to the defect

s - applied stress

u - threshold for POT

$A_{\max,V_E}$ - size of the prospective maximum defect in the volume V_E

C - constant

F - cumulative distribution function

$|J|$ - Jacobian determinant

K - stress intensity factor

N - number of fatigue cycles

N_E - number of elements

N_{IP} - number of IPs

$N_{k,\sigma}$ - knee-point of the Wöhler curve

P - applied force

P_f - failure probability

$\mathcal{R}$ - reliability

S_{ext} - external surface

V_E - generic material volume

V_{IP} - volume associate with an IP

V_{surf} - surface volume

V_0 - control volume for maxima sampling

Y - boundary correction factor for SIF calculation

ρ - defect density

ρ_u - density of the exceedances over a threshold u

σ_1 - maximum principal stress

ξ, η, ζ - non-dimensional parent element coordinates

ΔK_{th} - crack propagation threshold

$\Delta K_{\text{th,LC}}$ - crack propagation threshold for long cracks

$\Delta\sigma$ - applied stress range

$\Delta\sigma_{w0}$ - fatigue limit in the absence of defects

Σ - stress tensor

$\sqrt{\text{area}}$ - Murakami's defect size parameter

$\sqrt{\text{area}}_0$ - El-Haddad's material size parameter

Acronyms

cdf - cumulative distribution function

AM - additive manufacturing

CT - X-ray computed tomography

CV - coefficient of variation

FCG - fatigue crack growth

FE - finite element

GP - Gauss point

(V)HCF - (very) high cycle fatigue

IP - integration point

LCF - low cycle fatigue

MC - Monte Carlo

NDE - non-destructive evaluation

POT - peaks-over threshold

ROI - region of interest

SIF - stress intensity factor

SLM - selective laser melting

WL - weakest link

WS - witness sample

Subscripts

a - amplitude

chain - related to a prospective set of elements

cr - critical value

comp - related to the component

i, j - indices

max - maximum

w - related to the fatigue limit

A - related to the defect size

V_E - related to V_E

1. Introduction

In recent years, Additive Manufacturing (AM) techniques have been increasingly used for aerospace applications, due to the unique strengths of the additive processes. Although a large part of these applications is today limited to non-critical components, the spaceflight industry is aiming to extend the adoption of AM for structural applications. However, the qualification of AM structural parts needs a very costly and time-consuming series of fatigue tests, on both samples and full-scale parts. For these reasons, the development of rapid qualification techniques remains a matter of great interest to the AM community as part of the strategy to decrease product development time and cost, and therefore time to market new AM parts and components [1, 2].

The benefits and degrees of freedom offered by the technology are counterbalanced by some important drawbacks, e.g., poor surface roughness, ineluctable presence of manufacturing defects, material anisotropy. These variables influence the fatigue resistance by introducing large scatter in the material response [3]. Due to the strict reliability requirements for structural aerospace applications, a robust determination of the material fatigue resistance usually demands long and expensive experimental testing campaigns. Moreover, small variations in the manufacturing process can cause non-negligible differences in the fatigue strength of materials produced with the same alloy and machine [4]. For these reasons, a fast but robust approach for the fatigue design and verification of components containing defects is needed.

Aerospace safe life evaluation procedures assume that no anomalies are present in the material. This assumption would practically hinder all the applications of AM to critical parts, as defect-free components are almost impossible to be achieved with the current process maturity. In this context, the Federal Aviation Administration (FAA) foresees the use of damage tolerance to augment the current safe life approach [5]. Due to the random nature of anomalies, considering always the worst-case defect in the most critical location would not be feasible, and a probabilistic assessment comparing the failure probability to the allowable risk would be more suitable. The need for probabilistic frameworks is even clearer considering the many sources of scatter and the large number of variables involved [1, 2, 6, 7].

The first standard for the qualification of AM spaceflight hardware [8], developed by NASA, requires incorporating the sources of variability in the material characterisation and performing witness testing for every build. However, material validation alone is not sufficient, as components are more complex and can have non-negligible local differences [9], which is why full-scale

testing and proof-tests are required. Even if the full-scale part passes the test, there is no certainty that the following part will be safe. In fact, the very complex shapes that AM can produce (e.g., obtained by topological optimisation) suffer the drawback of containing small notched regions that work as stress raisers. For this reason, the failure probability is the probability that a large enough defect falls in a small but highly-stressed region. Given the impossibility to test enough parts to ensure the strict reliability requirements, the two options are verifying the specific part or ensuring a very low failure probability for the geometry and build of material investigated.

The fatigue strength of materials containing defects was addressed in '90's by Murakami and co-authors, who clearly showed that fatigue strength can be estimated as the threshold conditions for non-propagating cracks ahead of the inhomogeneities [10, 11]. Defects could be treated as short cracks and fatigue limit has to be estimated considering that the crack propagation threshold ΔK_{th} depends on defect size [10]. Moreover failure is driven by the most severe defects, i.e., the largest flaws in the most stressed material volume [12, 13].

A literature review on additively manufactured AlSi10Mg and Ti-6Al-4V has demonstrated that the presence of manufacturing defects (mostly pores and lack-of-fusion) and the dependence of fatigue strength on defect size are the main cause of scatter in fatigue data [14]. Following Murakami's concepts, the influence of defect size can be assessed by means of the Kitagawa diagram (Fig. 1a) by describing the defect dimension through the $\sqrt{\mathrm{area}}$ parameter (i.e., the square root of the area of the defect [13] as in Fig. 1b).

An extensive experimental investigation on the fatigue resistance of AlSi10Mg [4, 15] demonstrated these concepts by fatigue testing the same material produced by three Selective Laser Melting (SLM) processes, referred to as process 1 to process 3 (P1-P3). The results showed that the differences detected between the three S-N curves (see Fig. 1c) were mainly caused by the size of critical defects (Fig. 1d). Knowing the defect population, it was possible to evaluate the fatigue resistance in the fatigue limit region and estimate the trend and scatter of the data by fatigue crack growth (FCG) simulations (see the results obtained for P1 and P2 in Fig. 1c). The same concepts, which allow to better estimate the effect of defect size than concepts of stress concentration [16], were proven to be useful by other authors as well [17–19].

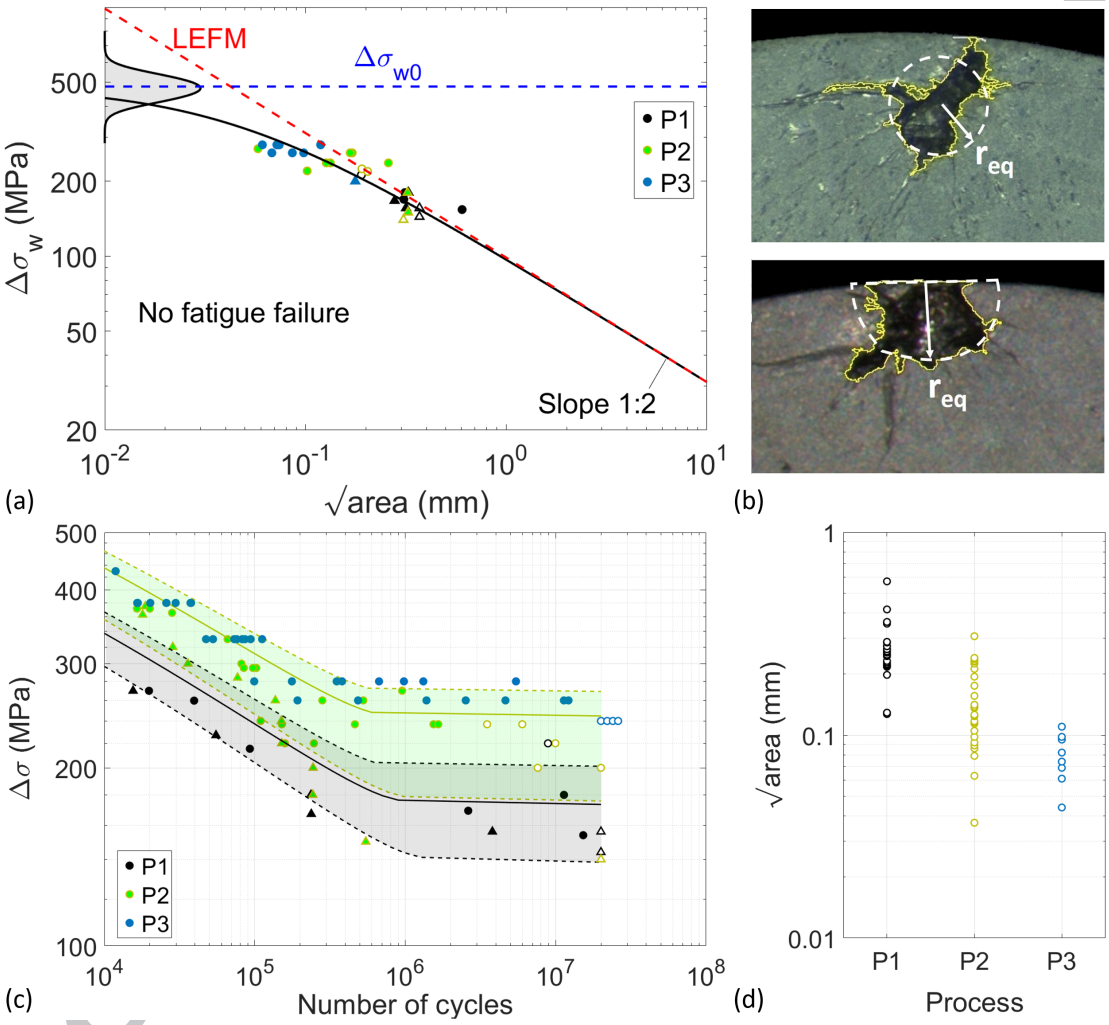

Figure 1: Resistance condition in the fatigue limit region: (a) fatigue strength as a function of defect size (Kitagawa diagram, adapted from [4]); (b) concept of $\sqrt{\text{area}}$. Influence of defect size on the fatigue resistance of AlSi10Mg produced by SLM (from [4]): (c) S-N curves and life estimations by FCG simulations for P1 and P2; (d) size of the killer defects.

1.1. Methods for probabilistic fatigue strength/life assessment

There is a general problem in fatigue, the effect of *component size* [20], which refers to the fact that fatigue properties tend to decrease when the size of the part increases (mainly in the case of unnotched test pieces [20]). This behaviour looks to be related to the probability of finding a *weak point* in the material microstructure and it has found a confirmation in the fatigue properties of metals containing defects [21] and in the static properties of ceramic materials [22].

The simplest probabilistic model for describing such an effect is the concept of *weakest link* (WL). Denoting by F_{chain} the cumulative distribution function (cdf) for a chain composed by N_E elements, under the hypothesis of independent elements, it can be written as

$$\mathcal{R}_{\text{chain}} = 1 - F_{\text{chain}} = \prod_{j=1}^{j=N_E} (1 - F_j) = \prod_{j=1}^{N_E} \mathcal{R}_j, \tag{1}$$

where $\mathcal{R}$ denotes the reliability ($\mathcal{R} = 1 - F$) and F_j is the cumulative distribution function for the elements. This equation allows to model the dependence of fatigue properties on size and it can be easily handled if F is expressed by the Weibull distribution [23]. This concept has been applied for expressing the size dependence of fatigue strength for cast materials [24] and high strength steels [21]: in these analyses, the volume (or surface) of a material element was considered to be composed by N_E volume (or surface) reference elements.

The same approach can be adopted for describing the reliability of a component $\mathcal{R}_{\text{comp}}$ discretised by a set of N_E independent material elements subjected to different stresses as

$$\mathcal{R}_{\text{comp}} = \prod_{j=1}^{N_E} \mathcal{R}_{V_E,j}, \tag{2}$$

where $\mathcal{R}_{V_E,j}$ expresses the reliability of the j_{th} material element of the discretisation subjected to the stress s_j. Based on this concept, different papers adopted this scheme for expressing the *notch effect* in fatigue adopting the Weibull distribution [21, 25].

The adoption of the WL to finite elements was firstly discussed in [26] based on the Weibull distribution: the concept of *weakest-link* applied to finite elements was mathematically developed by referring to a discretisation in volumes or surfaces (volume elements or surface elements) as **two separate models** for describing the size effect. A similar approach was also recently adopted by Schmitz et al. [27] for describing the size effect in low cycle fatigue (LCF). This analysis demonstrated that a formulation based on surface was more suitable for fatigue assessment of Ni-based superalloys.

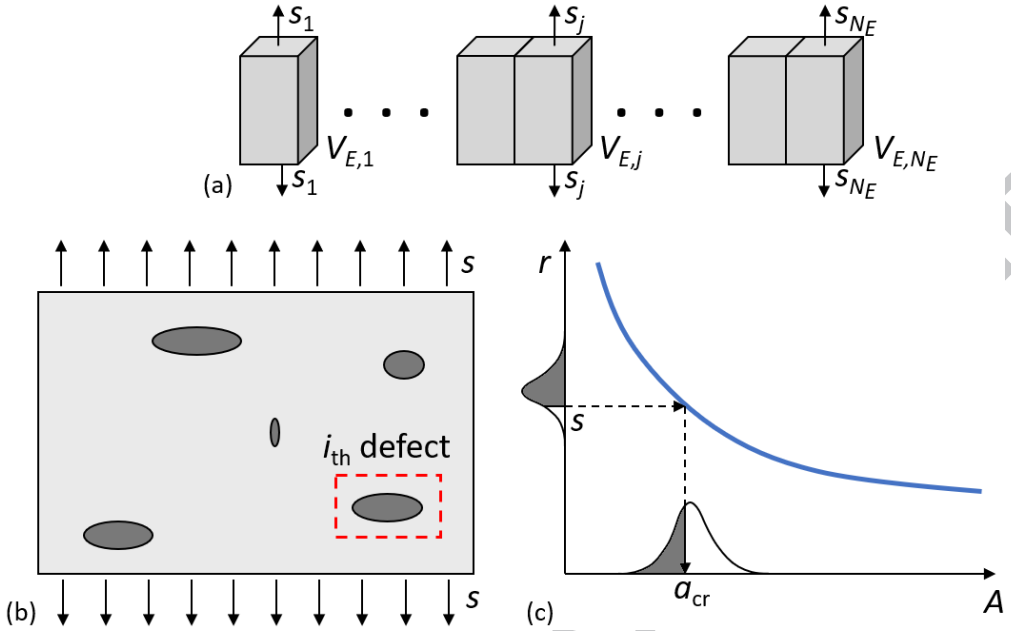

Figure 2: Basic concepts of Pro-FACE: (a) ideal discretisation of an elastic problem into a set of j independent material volumes $V_{E,j}$; (b) schematics of a volume element containing defects; (c) calculation of the reliability $\mathcal{R}_i$ for the i_{th} defect.

The WL was firstly adopted for determining the fatigue strength in the presence of defects by Beretta et al. [28], who investigated components discretised in finite elements (FEs) by considering a constant stress (corresponding to the stress at the centroid) within every finite element and adopting the strength model by Murakami-Endo [10]. The calculation was performed under the conservative hypothesis that all defects could be treated as *surface cracks*.

The FE formulation of the WL for probabilistic analysis of components containing defects was then fully developed mathematically at NTNU by the research group headed by G. Härkegård and implemented in the software P-FAT [29]. This formulation is based on the El-Haddad model and on describing the maximum defect size in material volumes through an extreme value distribution function. The authors demonstrated that the fatigue strength distribution could be described by a Weibull function, and applied the WL concept to evaluate the failure probability of components. However, the approach performed no distinction between surface or internally located defects and it was only mentioned that the same WL formulation was also applied to surface features (roughness, free surface grains, defects close to the surface). Moreover, the ana-

lytical version of P-FAT was not able to provide estimates of the fatigue life.

In order **to circumvent these two problems**, a new **explicit** version of P-FAT was developed at NTNU, where the WL concept and the analytical calculations were substituted by explicit and direct FCG calculations for a set of defects randomly located in the component. The distributions of fatigue strength (or fatigue life) were then obtained through Monte Carlo (MC) simulations [30, 31].

A similar **explicit** approach is adopted inside the simulation software DARWIN [32], developed by SWRI. DARWIN was initially developed for the certification of turbine engine disks [33–35]. The current version of the software is able to analyse 3D components with inherent flaws and defects: probabilistic FCG analyses are performed by extensive MC simulations by placing anomalies in every FE node and applying the WL theory. The fatigue strength distribution is obtained from the distribution of failure probability for an infinite fatigue life. Other software exist for probabilistic analyses of turbine disks [36].

The **main problem** of explicit FCG calculations is the time needed for the crack growth analyses and MC simulations, which makes it difficult for a designer to rapidly explore the design space for dimensioning a **defect-tolerant** component subjected to cyclic loads.

This is the area of innovation of the **Pro-FACE** (**Pro**babilistic **F**atigue **A**ssessment of **E**ngineering **C**omponents with d**E**fects) software. This tool, whose features are compared with those of similar software in Tab. 1, was conceived as a quick probabilistic instrument able to support the design of AM components.

	Analytical	Defect location	Fully probabilistic	Stress gradient
DARWIN		x		x
P-FAT explicit		x		x
ASTRID (2D)		x	x	x
P-FAT analytical	x			
Pro-FACE	x	x	x	*

Table 1: Summary of the main capabilities of the computational tools available (* currently under investigation).

The paper describes the concept of the software, its validation and an application as follows. In Sec. 2 are introduced the idea and the mathematical formulation lying at the root of the model, as well as the important input necessary for a proper probabilistic assessment. The convergence and performance are verified by MC simulations and validated by state-of-the-art FCG simulation. The capability of Pro-FACE to deal with complex parts is finally demonstrated considering a space component.

2. Theoretical background

2.1. Basic concepts

The reliability $\mathcal{R}$ of a material volume V_E that contains n defects and is subjected to the constant stress s (as in Fig. 2b) can be expressed as

$$\mathcal{R}_{V_E} = \Pr[r > s], \tag{3}$$

where r is the material resistance. Most of the approaches in the literature for such problem are based on the WL concept, that is

$$\mathcal{R}_{V_E} = \prod_{i=1}^{n} \mathcal{R}_i = [\mathcal{R}_i]^n, \tag{4}$$

where

$$\mathcal{R}_i = \Pr[r_i > s] \tag{5}$$

is the reliability of material surrounding the i-th defect (Eq. 5).

The usual approach for the WL analysis is to express $\mathcal{R}$ with a suitable distribution function and then calculate $\mathcal{R}_{V_E}$ as a function of the volume V_E. Alternatively, the i-th strength r_i can be written as a function of the defect size a in terms of linear elastic fracture mechanics or adopting the *short-crack theory*, i.e.

$$r_i = r(a_i), \tag{6}$$

where $r(a)$ is a suitable material resistance model, able to express the dependence on defect size a. The reliability of the i-th defect is then determined as in the scheme of Fig. 2c:

$$\mathcal{R}_i = F_A(a_{\mathrm{cr}}), \tag{7}$$

where F_A is the cdf of the defect size and

$$a_{\mathrm{cr}} = r^{-1}(s) \tag{8}$$

is the critical defect size for the stress s, i.e., the initial size of the critical crack.

In the field of fatigue strength in the presence of defects, s represents the stress amplitude and a is the defect size, which can be conveniently expressed by Murakami's $\sqrt{\text{area}}$ parameter [14]. The function r in Eq. 6 can be defined through the modified El-Haddad model of the $\sqrt{\text{area}}$ model developed by Murakami & Endo [10].

The alternative approach to express the fatigue strength as a function of material volume is based on *statistics of extremes* and consists in calculating the reliability of the volume V_E as

$$\mathcal{R}_{V_E} = \Pr[A_{\max,V_E} < a_{\text{cr}}] = F_{A_{\max,V_E}}(a_{\text{cr}}), \tag{9}$$

where $A_{\max,V_E}$ is the size of the prospective maximum defect in V_E. This can be mathematically expressed as [37]

$$F_{A_{\max,V_E}}(a) = [F_A(a)]^n. \tag{10}$$

The equivalence of the alternative approach to the WL can then be simply verified:

$$F_{A_{\max,V_E}}(a_{\text{cr}}) = [F_A(a_{\text{cr}})]^n = [\mathcal{R}_i]^n. \tag{11}$$

When adopting the concepts of *statistics of extremes* for analysing the defects, it is customary to estimate the distribution of the maximum defect on a *control volume* V_0 related to the sampling procedure [12, 38–40]. Accordingly, the reliability of the volume V_E can be written as

$$\mathcal{R}_{V_E} = [F_{A_{\max,V_0}}(a_{\text{cr}})]^{V_E/V_0}. \tag{12}$$

The model, originally proposed by Beretta [41], has been applied to components discretised in FEs by considering a constant stress (corresponding to the stress at the centroid) within every FE [28, 42].

2.2. Extension to a domain discretised by finite elements

The alternative approach, based on the *extreme value distribution* of the maximum defects, can be further extended to a material volume V_E whose stress field is not uniform. This allows to apply the model inside a post-processor of FE analyses.

The reliability of a material volume V_E subdivided into small sub-volumes dV can be calculated through a WL (or a series system) of the sub-volumes by re-writing Eq. 12 as

$$\log \mathcal{R}_{V_E} = \sum_{V_E} \frac{dV}{V_0} \cdot \log \left[F_{A_{\max,V_0}}(a_{\text{cr}})\right]. \tag{13}$$

Under the hypothesis of vanishingly small dV, Eq. 13 becomes

$$\log \mathcal{R}_{V_E} = \frac{1}{V_0} \int_{V_E} \log \left[F_{A_{\max,V_0}}(a_{\mathrm{cr}}) \right] dV. \tag{14}$$

By defining the function $Z(x,y,z) = \log \left[F_{A_{\max,V_0}}(a_{\mathrm{cr}}(s(x,y,z))) \right]$, the integral in Eq. 14 can be written by mapping the volume V_E onto the iso-parametric coordinates (ξ, η, ζ)

$$\int_{V_E} Z(x,y,z) dV = \int_{V_E} Z(x,y,z)\, dx\, dy\, dz = \int_{\xi}\int_{\eta}\int_{\zeta} Z(\xi,\eta,\zeta)\, |J|\, d\xi\, d\eta\, d\zeta, \tag{15}$$

where $|J|$ is the determinant of the Jacobian matrix.

This integral can be approximated with the typical numerical method adopted in FE codes (i.e., N-point Gauss quadrature [43]) as a triple summation evaluated at the integration points (IPs) and weighted accordingly:

$$\int_{\xi}\int_{\eta}\int_{\zeta} Z(\xi,\eta,\zeta)\, |J|\, d\xi\, d\eta\, d\zeta \simeq \sum_{i=1}^{N}\sum_{j=1}^{N}\sum_{k=1}^{N} Z(\xi_i,\eta_j,\zeta_k)\, |J|\, w_i\, w_j\, w_k, \tag{16}$$

where $(\xi_i = \eta_i = \zeta_i, w_i)$ are Gauss abscissae and weights. At each integration point IP_{ijk} at $(\xi,\eta,\zeta) \equiv (\xi_i,\eta_j,\zeta_k)$ the volume $V_{\mathrm{IP}_{ijk}} = |J|\, w_i\, w_j\, w_k$ can be associated, such that

$$V_E = \sum_{i,j,k=1}^{N} V_{\mathrm{IP}_{ijk}},$$

$\sum_{i,j,k}$ being a shorthand notation for the triple summation $\sum_i \sum_j \sum_k$.

The approximate solution of Eq. 14 can be calculated evaluating the stress $s_{\mathrm{IP}_{ijk}}$ at every IP_{ijk} as

$$\log \left\{ \mathcal{R}_{V_E} \right\} = \left\{ \frac{1}{V_0} \sum_{i,j,k=1}^{N} Z(s^*_{\mathrm{IP}_{ijk}}) \cdot V_{\mathrm{IP}_{ijk}} \right\}. \tag{17}$$

If the WL concept is applied to a component discretised in N_E FEs having a volume $V_{E,j}$, the final reliability is

$$\mathcal{R}_{\mathrm{comp}} = \prod_{j=1}^{N_E} \mathcal{R}_{V_{E,j}}, \tag{18}$$

or

$$\log \mathcal{R}_{\mathrm{comp}} = \sum_{j=1}^{N_E} \log \mathcal{R}_{V_{E,j}}, \tag{19}$$

where the reliability of the j-th finite element can be calculated through Eq. 17.

2.3. Stress multiaxiality

The propagation of cracks from defects, such as non-metallic inclusions and pores, tends to grow in a direction perpendicular to the (local) maximum principal stress range [30]. In fact, this is the preferred growth orientation of fatigue cracks beyond microstructural size scales (i.e., mode I cracks) [44]. This hypothesis is adopted in most fatigue models dealing with defects (e.g., DARWIN, P-FAT), and is also exploited in the present model. In details, considering multiaxial conditions, Beretta and Murakami [45] showed that the fatigue limit, in terms of stress amplitude for the maximum principal stress under in-phase multiaxial loading, is

$$r_{\text{multiaxial}} = r(a) \cdot f\Big(\frac{s_{1,a}}{s_{3,a}}\Big), \tag{20}$$

where $s_{1,a}$ and $s_{3,a}$ are respectively the maximum and minimum principal stresses $r(a)$ is the function expressing the Kitagawa diagram and $f(\frac{s_{1,a}}{s_{3,a}})$ accounts for the effect of stress multiaxiality (e.g. $f(-1) = 0.85$ under torsion) [45]. This equation was adopted for calculating the critical crack size at any IP based on the local stress tensor Σ.

3. Implementation of Pro-FACE

3.1. Surface effects

In a real 3D body, the defect position significantly affects the stress intensity factor. In fact, the shape factor is considerably different for surface and internal defects, which makes surface cracks more detrimental than internal ones. By describing the defect size according to the $\sqrt{\text{area}}$ parameter, the stress intensity factor (SIF) can be calculated as [13]

$$K = Y \cdot \sigma \cdot \sqrt{\pi \cdot \sqrt{\text{area}}}, \tag{21}$$

where the boundary correction factor is set to $Y = 0.65$ for surface defects or $Y = 0.5$ for internal defects.

A simple rule proposed by Murakami [13] states that a defect can be considered superficial when

$$r_{\text{eq}}/h > 0.8, \tag{22}$$

where r_{eq} is the radius of the equivalent circle (a circle having the same area as the defect) and h is the distance between the defect centre and the outer surface (see a scheme in Fig. 3a). In a given material volume, the maximum size of the largest defect ($a_{\max}$) depends on the reference volume V_E according to Eq. 12. It is then clear from Eq. 22 that the depth h above which a

defect can be considered as internal is a function of the shape of the volume under investigation. Calling S_{ext} the external surface of the material volume, the distribution of the maximum defect located in the surface region can be approximated as the one occurring in a *surface volume*

$$V_{\text{surf}} = S_{\text{ext}} \cdot h. \tag{23}$$

These concepts have been applied to cylindrical fatigue specimens [46] setting r_{eq} in Eq. 22 equal to the average size of the defects from which fatigue failures were originated. A scheme of the surface volume thus obtained is depicted in Fig. 3b.

More generally, the problem of determining h is similar to the so called Wicksell's problem about inferring the distribution of 3D defects from 2D planar sections [47, 48]. The determination of h can be solved recursively, without the need for experimental results, depending on the part shape (ratio surface/volume) and defect distribution. Once the value of h is determined, the distinction between surface and internal IPs in a FE environment can be evaluated based on the distance of these points from the outer surface, as in Fig. 3c.

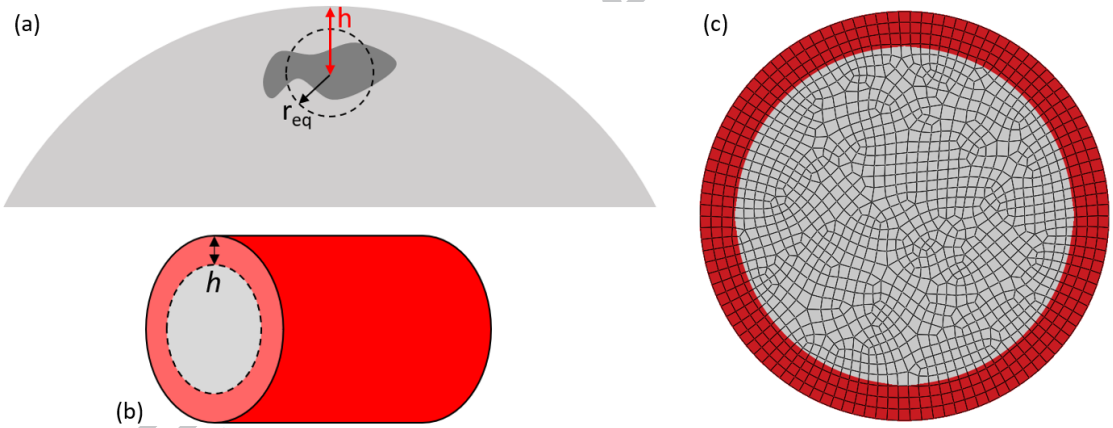

Figure 3: Definition of the surface volume: (a) surface defects according to Murakami [13]; (b) scheme for a cylindrical specimen; (c) assessment with a FE mesh.

A comparison of different computations of h for notched components was discussed in [49], where a conservative solution was proposed that depends on the component under investigation. Pro-FACE considers as superficial all the material having a distance from the external surface smaller than h, while all the other IPs are treated as internal. The SIF calculation and Y factors are calculated as in Eq. 21. The importance of considering the surface effects are described in Sec. 5, which presents the results obtained investigating a notched geometry through the method developed.

3.2. Implementation

The idea underpinning the model is to evaluate the reliability as the probability that the SIF acting on every defect is smaller than the short cracks propagation threshold (defined by the Kitagawa diagram), i.e., that fatigue crack propagation is hindered. Therefore, the model was initially designed to assess the fatigue limit of the parts (or more in general the fatigue strength in the high cycle fatigue (HCF) and very high cycle fatigue (VHCF) regimes, always above the knee-point of the S-N curve). The inputs required for the assessment are:

1. a FE analysis of the part;
2. a suitable description of the defect population;
3. a model for material resistance in the presence of defects.

The FE analysis requires no effort, as it is commonly performed for all industrial applications. The output data needed are the maximum principal stress and the volume on which every stress computed is acting.

The defect population can be obtained by destructive or non-destructive testing on the material (witness samples for the design phase) or, if possible, directly on the component to be qualified by NDE. The two ingredients to obtain a proper distribution are to consider all the defect sizes meaningful for fatigue and to precisely model the upper tail of the data [46].

The material resistance in the HCF and VHCF region can be evaluated by means of the Kitagawa diagram, which is defined for a given life [4] or estimated by elastic-plastic FCG models [15].

A scheme summarising the root concept is depicted in Fig. 4. The critical defect size for the material volume under investigation is defined by entering the Kitagawa diagram with the applied stress. The reliability is the probability that the maximum defect (expressed as the maximum defect size distribution in the volume considered by means of statistics of extremes) is smaller than the critical size. The mesh adopted for the FE analysis is exploited by performing the computations on all the IPs. This ensures the adoption of the correct applied stresses, instead of the results averaged at nodes. Finally, the component failure probability (P_f) is determined by a WL approach.

The model presented has been implemented in a series of routines for the post-processing of FE results based on the equations reported in Sec. 2. The method described has the advantage of

being completely analytical, thus running very fast also on complex and heavy FE models. Furthermore, provided that the stress field is correctly solved by the FE analysis (i.e., a proper mesh needs to be adopted), the result is mesh-insensitive and therefore only application-dependent.

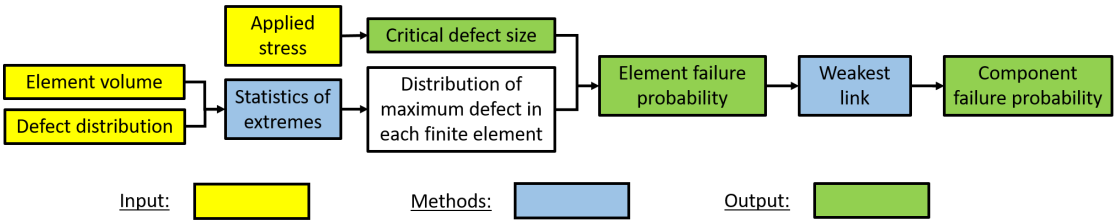

Figure 4: Implementation of Pro-FACE: concept of the probabilistic analysis.

3.3. Validation by Monte Carlo simulations

There are two key elements for a proper determination of the reliability with Eq 14: (i) a correct calculation of the integral of the function Z (Eq. 15) with Gaussian discretisation and (ii) the convergence of this quantity in respect of that of the reconstructed stress field. The discussion related to point (i) is reported in AppendixA, whereas the convergence of the model was tested with a series of Monte Carlo simulations on a simple geometry.

The geometry selected to evaluate the response to a stress gradient is an infinite plate with a central hole subjected to a uniaxial tension s. This geometry allowed to know a-priori the analytical solution of the stress field (according to the theory of elasticity [50]), which is reported in Fig. 5a in terms of maximum principal stress. The plate dimensions are 40 mm x 40 mm, whereas the central hole radius measures 1 mm. These values guarantee a negligible difference caused by the finite dimensions of the FE model with regard to the analytical solution of an infinite plate. As shown in the scheme in Fig. 5a, the symmetries of the problem have been exploited by modelling one fourth of the plate.

The reference value for the P_f was obtained by MC simulations. The steps needed for this analysis are summarised here:

1. 2/3D defect generation inside the control area/volume using a Poisson process [51, 52], defining number and position of the defects;

2. defect size calculation by MC extraction, given the defect size distribution in terms of $\sqrt{\text{area}}$;

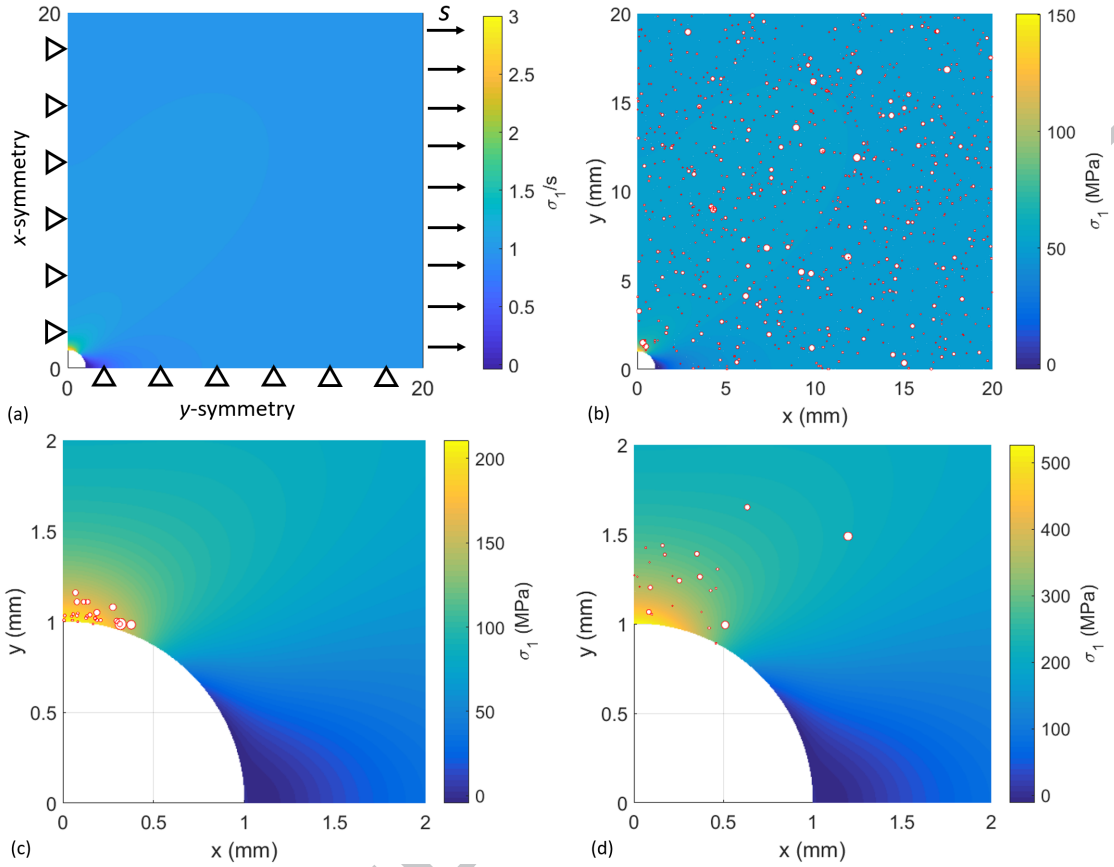

Figure 5: Failure probability calculation by MC simulations: a) schematics of the plate with a hole; b) example of defects sampled in one simulation; critical defects obtained by 100 simulations with (c) low applied stress and high defect density or (d) high applied stress and low defect density.

3. assessment of the critical defect size ($\sqrt{\text{area}}_{\text{cr}}$) inside the Kitagawa diagram based on the analytical stress field evaluated at the centre of every defect generated (the material data for AlSi10Mg P1 taken from [4] were used, see Sec. 4.1);
4. determination of the failure probability for every k-th simulation: $P_{f,k} = 1$ if the relationship $\sqrt{\text{area}} \geq \sqrt{\text{area}}_{\text{cr}}$ is verified for at least one defect, $P_{f,k} = 0$ otherwise;
5. repetition of the previous steps for a large number of simulations and final average of the failure probabilities obtained.

As an example, Fig. 5b shows the defects obtained in one of the simulations performed, which are depicted with a radius proportional to the $\sqrt{\text{area}}$ sampled. Fig. 5c-d shows the critical defects determined by running 100 MC simulations for two illustrating cases, in which the defect density

and remote stress s were selected to obtain in both cases a P_f of 50%. As expected, the most critical location corresponds to the most stressed region. However, this analysis demonstrates that all the three variables at stake (i.e., applied stress, defect size distribution, and defect density) can significantly influence the results.

Results by Pro-FACE model

To check the performance and convergence of the analytical model underscoring Pro-FACE, the problem was solved using three structured meshes with constant dimensions, summarised in Tab. 2.

Four types of bi-dimensional FEs were used, progressively increasing the number of IPs (see a schematic in Fig. 6a). Their characteristics are summarised in Tab. 3.

Number FEs	Mesh size (mm)
1600	0.5
6395	0.25
39937	0.1

Table 2: Summary of the three structured meshes adopted.

Name	Type	Integration	# of nodes	# of IPs
CPE4R	linear	reduced	4	1
CPE4	linear	full	4	4
CPE8R	quadratic	reduced	8	4
CPE8	quadratic	full	8	9

Table 3: Summary of the FE types investigated.

Pro-FACE considers the maximum principal stress at the IPs under the hypothesis that the whole IP volume is subjected to a constant stress. As discussed in AppendixA, this hypothesis could introduce errors in the presence of steep stress gradients and coarse mesh size. To verify how the model responds to this issue, the error made in the stress field reconstruction was evaluated in the most stressed point of the plate, which has coordinates (0,1). As shown in Fig. 5a, the maximum principal stress in this point is thrice the nominal one. Fig. 6b-c compares this value

respectively to the maximum stress reconstructed at that node and at the closest IP.

Performing many MC simulations ($3 \cdot 10^6$ for the case presented), the reference P_f for the component was computed and the 95% error band could be evaluated. Fig. 6d compares the target P_f with the results of the proposed analytical model, which were obtained considering the FE types and mesh sizes previously described.

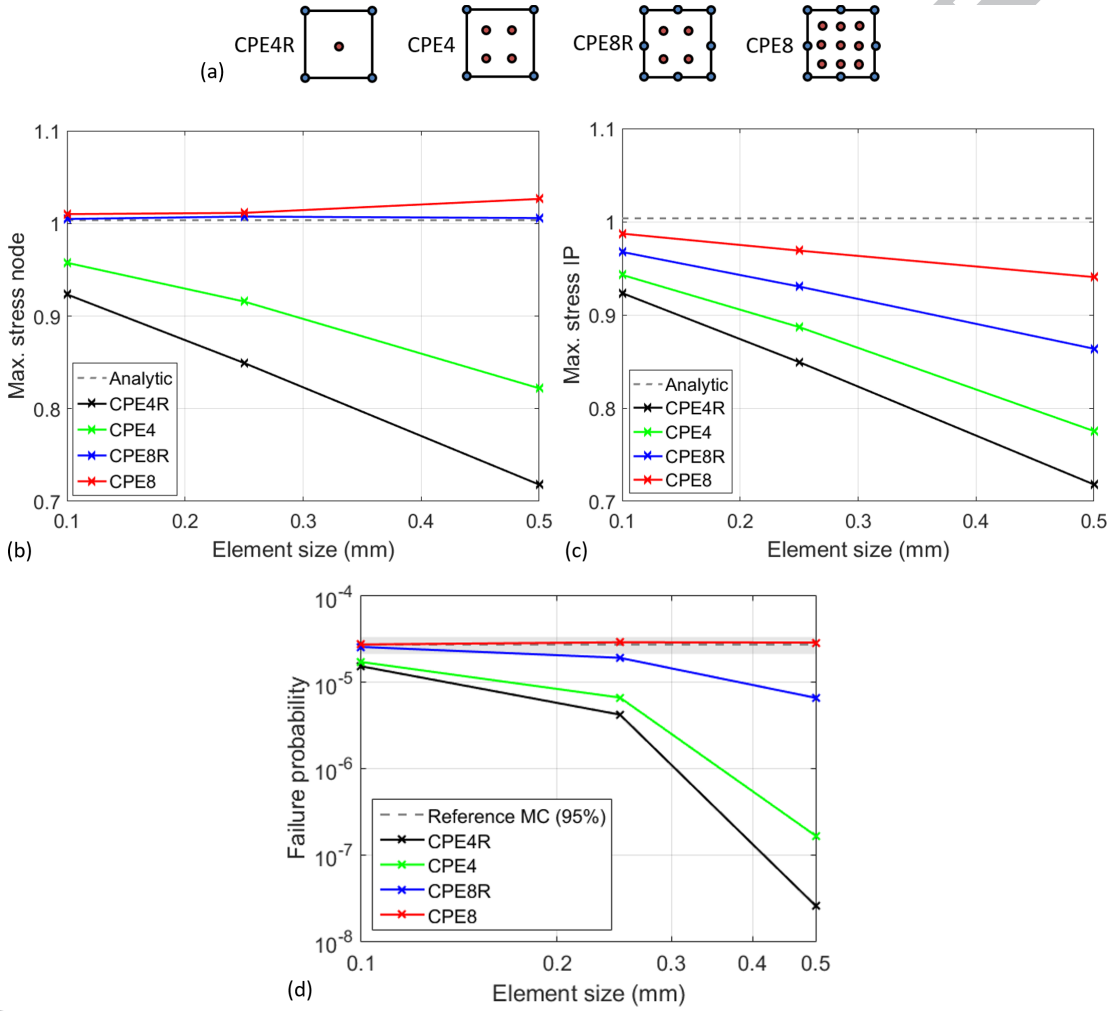

Figure 6: Convergence of the discretised FE model with regard to the reference solution (analytical for the stress, MC simulations for the P_f): (a) scheme of the FEs adopted; (b) maximum nodal stress; (c) maximum principal stress at the closest IP; (d) failure probability.

The picture shows that quadratic elements with reduced integration (CPE8R) give correct results

already with medium mesh sizes, whereas CPE8 elements show good convergence even with very coarse meshes. As expected, the poor results obtained by linear FEs in the presence of notches were confirmed. Note, however, that the error committed with a fine mesh is in general acceptable, as the order of magnitude is correctly estimated.

4. Important ingredients for the analysis

Three main ingredients are needed to perform an efficient and robust evaluation of real parts, i.e., a proper modelling of the occurrence of defects near the surface (discussed in Sec. 3.1), the description of the Kitagawa diagram, a simple method for finite life assessment and a comprehensive description of the main sources of variability involved.

4.1. Model for fatigue strength

As discussed in Sec. 1, the fatigue strength of materials containing defects has to be evaluated using a *short cracks* model, i.e. describing the dependence of ΔK_{th} or limit stress $\Delta\sigma_w$ on defect size [11]. Among the various possibilities adopted in the literature, the simplest approach is modelling the defect size according to the $\sqrt{\mathrm{area}}$ parameter and adopting the modified El-Haddad formulation 25 [4, 14, 53–55] where:

$$\Delta K_{th} = \Delta K_{th,LC} \sqrt{\frac{\sqrt{\mathrm{area}}}{\sqrt{\mathrm{area}} + \sqrt{\mathrm{area}}_o}} \tag{24}$$

that combined with Eq. (23) gives:

$$\Delta\sigma_w = \Delta\sigma_{w0} \sqrt{\frac{\sqrt{\mathrm{area}}_0}{\sqrt{\mathrm{area}}_0 + \sqrt{\mathrm{area}}}} \tag{25}$$

By this formulation, the fatigue strength $\Delta\sigma_w$ can be derived as a function of the parameters $\sqrt{\mathrm{area}}_0$ and $\Delta\sigma_{w0}$ and of the defect size (Eq. (27) can be inverted for calculating $\sqrt{\mathrm{area}}_{\mathrm{cr}}$ at any IP). Alternatively, the threshold condition for a short crack can also be obtained by threshold formulations based on elastic-plastic *crack driving force* [15, 56].

4.2. Extension for finite life

In this section, the model presented based on the fatigue strength in the fatigue limit region is extended to finite life assessment. The finite life of a material volume for a given applied stress can be evaluated knowing the Kitagawa diagram and the Wöhler curve of the material. The latter can be expressed in terms of negative inverted slope k_σ and number of cycles corresponding to the knee-point $N_{k,\sigma}$ [4]. The fatigue life for $N \leq N_{k,\sigma}$ is described by the exponential relationship in Eq. 26:

$$N\,\Delta\sigma^{k_\sigma} = \mathrm{const} \tag{26}$$

At the knee-point, Eq. 26 becomes Eq. 27.

$$N_{k,\sigma}\,\Delta\sigma_w^{k_\sigma} = \mathrm{const} \tag{27}$$

Equating Eq. 26 and Eq. 27, the ratio $\Delta\sigma/\Delta\sigma_w$ can be obtained:

$$\frac{\Delta\sigma}{\Delta\sigma_w} = \left(\frac{N_{k,\sigma}}{N}\right)^{1/k_\sigma} \tag{28}$$

In [4] it was shown that, if the S-N data of various processes (e.g., those depicted in Fig. 1c) are normalised in relation to the corresponding fatigue strength resistance defined by the Kitagawa diagram, all the data collapse onto the same curve (see Fig. 7a). The same evidence is also reported for different materials [18]. This demonstrates that the Kitagawa diagram is a suitable model for defining the influence of the defect size for finite life assessments as well. This evidence was also confirmed by evaluating the relationship between the initial defect size and applied stress for various lives by FCG simulations [15].

Therefore, substituting $\Delta\sigma_w$ defined by Eq. 25 in Eq. 28, a unique equation describing the relationship between critical defect size $\sqrt{\text{area}}_{\text{cr}}$, number of cycles to failure N and applied stress $\Delta\sigma$ is obtained. In this way, it is possible to calculate the critical defect size for a given life and applied stress (Eq. 29).

$$\sqrt{\text{area}}_{\text{cr}} = \sqrt{\text{area}}_0 \left\{ \left[\left(\frac{N_{k,\sigma}}{N}\right)^{1/k_\sigma} \cdot \frac{\Delta\sigma_{w0}}{\Delta\sigma} \right]^2 - 1 \right\} \tag{29}$$

This relationship describes the average trend, but the variability of the experimental data shows that the strength assessment cannot be performed on a deterministic base. Therefore, the intrinsic material variability remaining after the normalisation (depicted in Fig. 7a) cannot be neglected.

The performance and limitations of the approach presented are discussed in Sec. 5.3, where the results are analysed through a challenging case study.

4.3. Fully-probabilistic framework

The standard way of assessing the fatigue resistance of parts containing defects is to adopt a semi-probabilistic framework, i.e., considering deterministic load or resistance. Even if most of the scatter is due to the defect size, there are some other sources of variability that might not be negligible. Among them, the most important are the material resistance (Kitagawa diagram) and the applied load/stress.

Considering the resistance, the material manufactured by AM technology generally showed non-negligible variability in the Kitagawa diagram (e.g., 8-13% for SLM AlSi10Mg as in Fig. 1a). This dispersion can be regarded as an uncertainty of the model and of the parameters describing the fatigue strength as a function of the defect size. A simple modelling of this

scatter was performed by assuming that $\Delta\sigma_{w0}$ can be described by a log-normal distribution and preserving the shape of the Kitagawa diagram. This hypothesis was seen to be consistent with the experimental evidence of the Kitagawa diagram and of the normalised S-N curve [4].

The influence of the material resistance variability can be accounted by MC simulation. However, an analytical solution to the problem has been investigated to decrease the computational burden and avoid uncertainty. To comply with the hypotheses of the WL model, the component reliability has to be calculated as described in Sec. 2.2

$$\mathcal{R}_{\text{comp}} = \mathcal{R}_{\text{comp}}(\Delta\sigma_{w0}), \tag{30}$$

that is $\mathcal{R}_{\text{comp}}$ is conditioned on $\Delta\sigma_{w0}$. If this material parameter is described by the probability density function $f_{\Delta\sigma_{w0}}$, the reliability can be calculated as

$$\mathcal{R}_{\text{comp}} = 1 - \int_0^{+\infty} \mathcal{R}_{\text{comp}}(\Delta\sigma_{w0}) \cdot f_{\Delta\sigma_{w0}}(\Delta\sigma_{w0}) \cdot d\Delta\sigma_{w0}. \tag{31}$$

Fig. 7b shows how to calculate the component reliability in the presence of a variable material strength (red area). $P_{f,\text{comp}} = 1 - \mathcal{R}_{\text{comp}}$ is first assessed in the whole range of definition of the material resistance (blue curve on the top) and weighted for the probability of occurrence of the particular resistance $f_{\Delta\sigma_{w0}}$ as in Eq. 31. This integral can be numerically solved by standard quadrature algorithms, or using other suitable methods (e.g. *integral transform* [57] or MC simulations [58]).

The Kitagawa diagram in Pro-FACE is modelled as a log-normal distribution with a given scatter and the parameter $\sqrt{\text{area}}_0$ is kept constant as already assumed in [59]. Alternatively, other models can be adopted for describing the variability of the Kitagawa diagram [60]. In the same way, this approach can be used to introduce variability in the applied load, thus defining a *fully-probabilistic fatigue strength approach.*

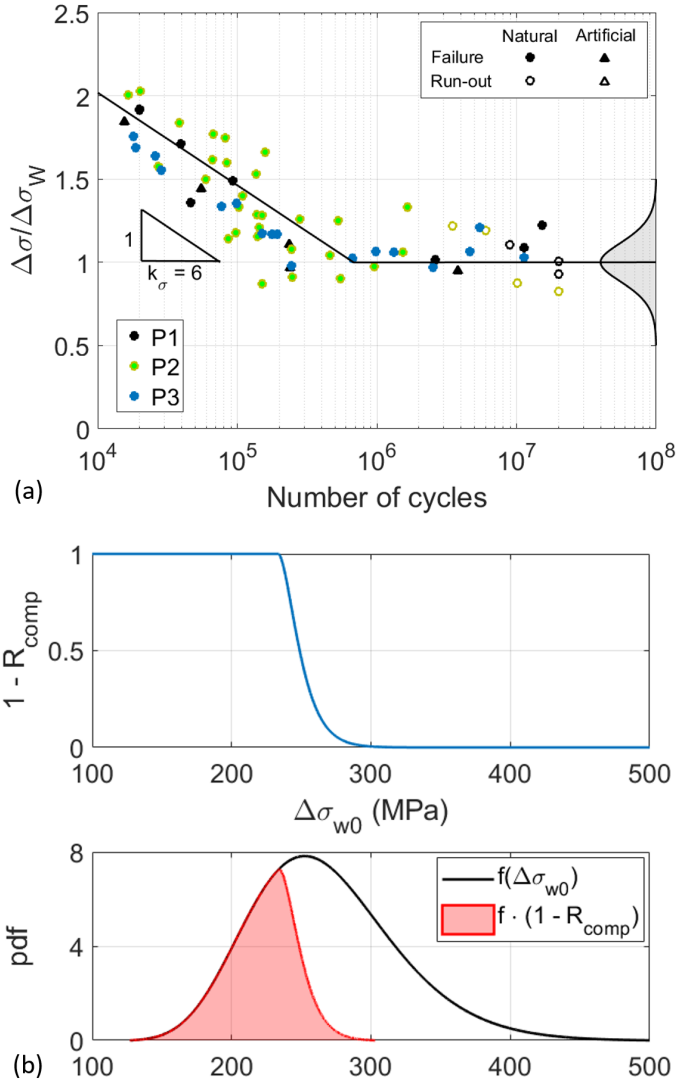

Figure 7: Ingredients for the analysis: (a) fatigue life assessment in the presence of defects by normalising the S-N curve with regard to the Kitagawa diagram (example data referring to the three processes depicted in Fig. 1a, figure adapted from [4]); (b) Scheme of failure probability calculation according to Eq. 31.

5. Validation on notched components

The results obtained with Pro-FACE were validated considering a notched sample. This geometry was chosen to verify the model predictions in the presence of notches and steep stress gradients. This activity was designed with multiple aims:

- verify the performance of the SIF-based defect criticality assessment [4] in the presence of stress gradients by considering all defects detected in the parts;
- validate the probabilistic assessment of the fatigue limit based on defect distribution and WL model with the results obtainable considering the most detrimental defects detected in the parts;
- compare the probabilistic life estimation to the deterministic results obtained performing state-of-the-art FCG simulations.

5.1. Samples design and details

In order to limit the number of unknown effects that could influence the results, the parts were designed choosing as simple a geometry as possible. Ten cylinders of 20 mm diameter and 155 mm length were built by SLM with horizontal orientation according to process P2. The samples were then machined to the final dimension according to the drawing in Fig. 8s. Two round notches were machined on the two sides to introduce high stresses in a limited material volume.

Computed tomography

X-ray CT and defect analysis were performed on all the samples. The tomography was performed setting a voxel size of 16 μm (see [46] for further details). A region of interest (ROI) was set considering a symmetric ± 15 mm material region in respect of the specimen centre, corresponding to the centre of the notches. An example of the size and position of the defects detected in this region considering specimen 1 is depicted in Fig. 9a. The relevant variables for the ten samples analysed are summarised in Tab. 4, where ρ is the defect density, ρ_u is the density of the exceedances above a threshold $u = 0.15$ mm, and $\sqrt{\text{area}}_{\text{max}}$ is the maximum defect size detected. The results showed a large variability in the defect densities, which ranged from 2 def/mm^3 to almost 80 def/mm^3, whereas the density of the defects larger than u was approximately two orders of magnitude smaller. The maximum defect size ranged from 0.222 to

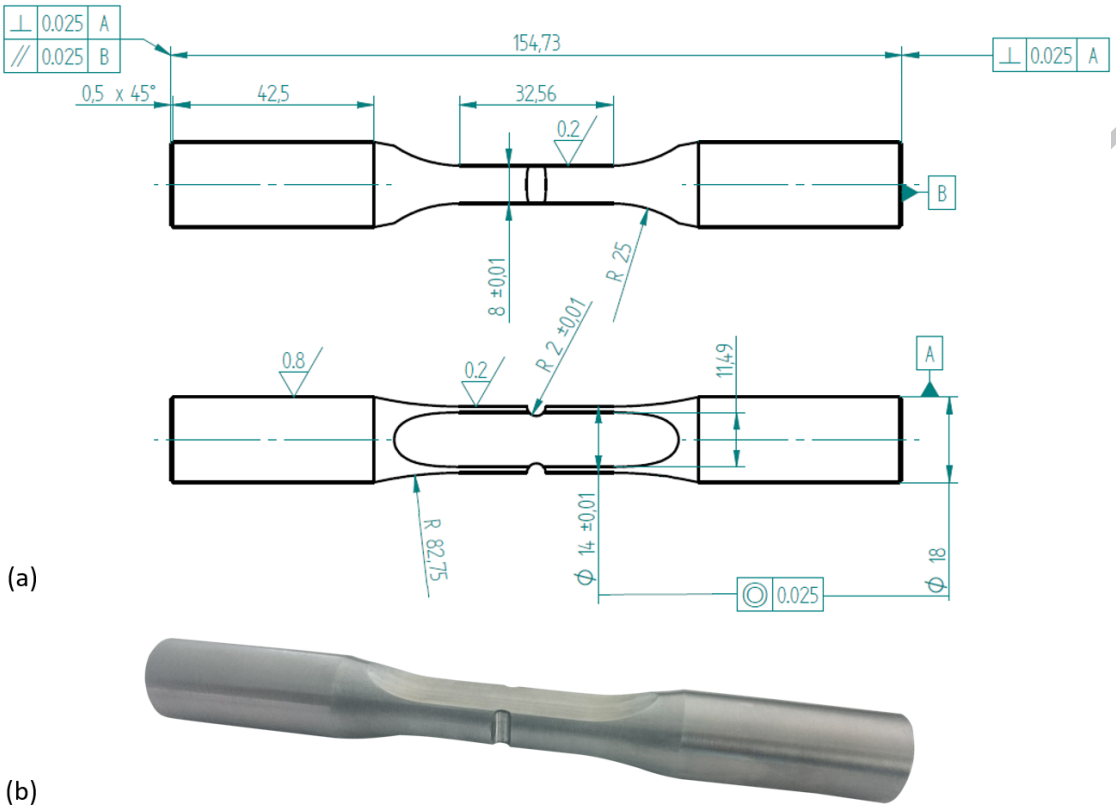

Figure 8: Notched part geometry: (a) technical drawing; (b) final part.

0.528 mm. Hereunder, specimen 1 will be considered as witness sample for the whole batch of parts.

Defect distribution

The defect distributions were fitted through a proprietary technique developed at PoliMi and used inside Pro-FACE. This method adopts a robust and simple analytical relationship able to describe the whole range of defect sizes detected. On the one hand, a proper modelling of the largest defects is the most important step, which was achieved by applying the method based on peaks-over threshold (POT) maxima sampling described in [46]. On the other hand, small defects can become more detrimental than large ones when placed in the most stressed locations in notched components. Therefore, they cannot be neglected for the present case-study. The technique adopted is able to describe both regions by *mixing* the two distributions [40]. This method consists in calculating the cumulative probability assigning a larger weight to the distribution of small defects for dimensions below the threshold, and larger weight to the

Specimen	ρ (def/mm^3)	ρ_u (def/mm^3)	$\sqrt{\text{area}}_{\text{max}}$ (mm)
1	15.39	0.154	0.528
2	78.33	0.396	0.518
3	35.55	0.241	0.510
4	38.95	0.257	0.376
5	73.93	0.149	0.359
6	6.08	0.039	0.370
7	13.60	0.030	0.309
8	17.95	0.087	0.379
9	1.98	0.012	0.222
10	11.89	0.044	0.486

Table 4: Relevant variables resulting from the defect analyses on the samples.

negative exponential distribution describing the exceedances above the threshold for larger defect sizes. An example of the final data fit achieved for specimen 1 is depicted in Fig. 9b.

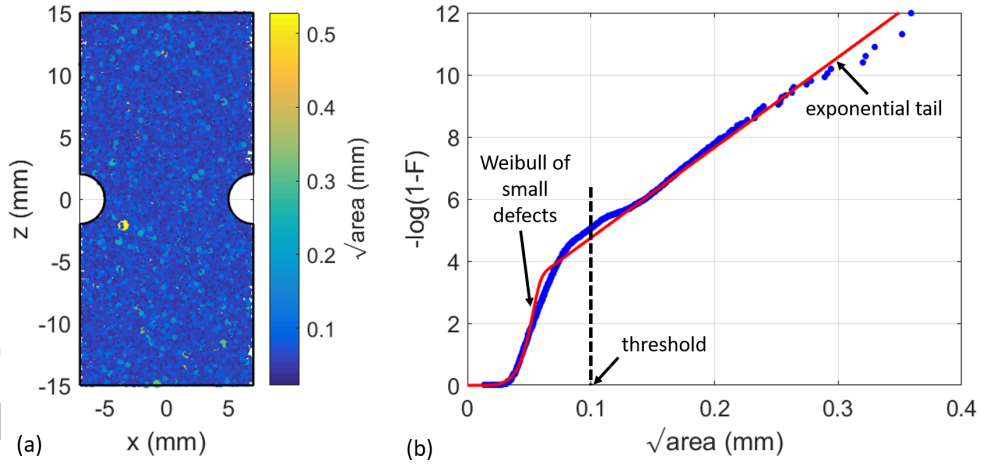

Figure 9: Example of defect distribution in the samples: (a) size and position of the defects detected; (b) analytical description of CT measurements.

FE model

The three symmetries along the principal axes were exploited by modelling only 1/8 of the sample in Abaqus 6.14. A fine quadratic mesh consisting of 23331 C3D20 elements was adopted to ensure the stress convergence, with mesh refinement around the notch. The load applied was an axial force $P = 6.8$ kN. The model and FE results are depicted in Fig. 10. The stress concentration factor at the notch tip was $K_t = 2.26$, with a 90% volume $V_{90} = 0.98$ mm^3 (i.e. the volume subjected to a stress larger than 90% of the maximum one).

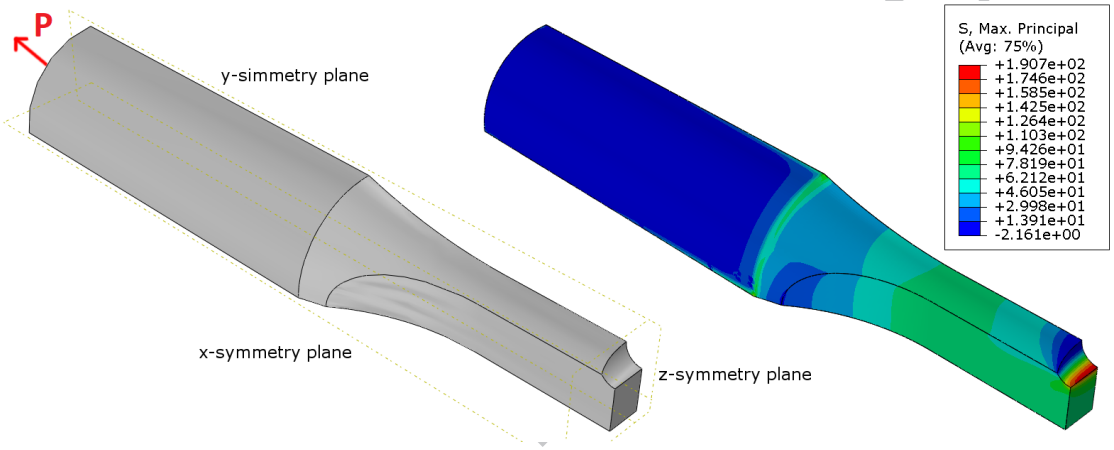

Figure 10: FE model of the part: geometry, loading condition and maximum principal stress results.

Model for material fatigue strength

The fatigue properties of the material manufactured by process P2 were completely characterised on the standard specimens built in the same built job (see [4, 46]). The results needed for Pro-FACE are the slope k_σ and knee-point $N_{k,\sigma}$ of the Wöhler curve, and the Kitagawa diagram described by the El-Haddad formulation (see Sec. 4.1-4.2). The intrinsic material variability not due to the defect size can be a further input for the probabilistic analysis. It can be expressed in terms of coefficient of variation (CV) of the fatigue data. Tab. 5 summarises the input data.

5.2. Results

The model validation was performed by a step-by-step process investigating two key points:

1. **prospective fatigue limit** of the notched specimens subjected to fully reversed axial fatigue loading;
2. **finite life** under a cyclic fully-reversed load with amplitude of 6.8 kN.

Wöhler curve	k_σ	6
	$N_{k,\sigma}$	$2 \cdot 10^5$
Kitagawa diagram	$\Delta\sigma_{w0}$ (MPa)	480
	$\sqrt{\text{area}}_0$ (mm)	0.038
Intrinsic material variability	CV	0.1

Table 5: Summary of the experimental fatigue results for process P2 (from [4]).

These two analyses were performed by adopting two types of assessments:

- a *deterministic approach*, which required performing CT on all parts to determine size and position of all major defects. The defects were then ranked by criticality according to their SIF, which was calculated by Eq. 21 based on the evaluation of the stress applied to any position of the sample obtained through FE analysis;
- Pro-FACE's *probabilistic approach*, which evaluates the probability of finding a critical defect in any location based on the defect distribution in the witness sample.

The results obtained for the finite life assessment were finally validated by state-of-the-art FCG simulations using the NASGRO 4.2 software.

Fatigue limit assessment

The deterministic approach consisted in evaluating the maximum allowable stress inside the Kitagawa diagram for the defect subjected to the maximum SIF, and thus the limit applicable load P_w. This required the development of a tool that could interface CT and FE results to assess the stress acting on every defect and the position with regard to the outer surface. This information is necessary to evaluate the defect criticality ranking.

The position of the most critical defect detected in each sample is represented in Fig. 11a, which also shows the expected criticality of the notch region evaluated by Pro-FACE in terms of normalised failure probability $P_{f,\text{norm}}$. Note that the size of the circles depicted is proportional to the $\sqrt{\text{area}}$ of the defects measured by CT, but scaled for visualisation reasons. The quantity $P_{f,\text{norm}}$ gives a qualitative and visual assessment of the zones in which the fatigue crack is likely to originate and a quantitative evaluation of the relative difference of failure likelihood among various positions.

By evaluating P_w for the ten samples investigated, the fatigue limit distribution depicted by the red dots in Fig. 11b-c was estimated. The same analysis was then performed with Pro-FACE refining the calculation step-by-step. The first assessment made the simplified assumption to consider all the IPs as superficial (grey dashed curve in Fig. 11b). The second simulation (black dotted curve) adopted the refined method implemented in Pro-FACE to distinguish surface and internal IPs (see Sec. 3.1). The third simulation (blue solid curve) exploited the capability of Pro-FACE to consider the intrinsic material variability, which was expressed by a 10% CV on $\Delta\sigma_{w0}$. In this case, the slope of the cdf decreases compared to the previous ones, which causes a larger scatter of P_w. Moreover, as CT analyses highlighted important variability in the defect density among the specimens, a worst-case and a best-case assessment were performed considering the largest and lowest defect densities measured (see Tab. 4), which are depicted by the blue semi-transparent region in Fig. 11b.

Finally, Fig. 11c shows how the most stressed volume affects the overall part assessment. The blue curve reported in Fig. 11a is compared here to the results obtained by performing the same assessment considering only the most stressed part of the sample, i.e., setting automatically $P_f = 0$ to all the IPs subjected to a stress lower than a given threshold. This analysis was performed considering V_{90} and V_{80}, which correspond to the component volumes subjected to at least 90% or 80% of the maximum principal stress applied (0.0019% and 0.0081% of the overall volume of the sample).

By comparing the results of deterministic and probabilistic approaches, it can be affirmed that all critical defects are placed inside the region associated with the largest criticality, very close to the surface of the notch. This was also demonstrated by the fact that the error committed basing the assessment exclusively on V_{90} is really small, and it becomes negligible considering V_{80} (see Fig. 11c). This result is in accordance with the findings reported in the literature [25, 61, 62], and highlights that the failure of notched parts is usually driven by very small volumes of material, and that the quality of these regions has a paramount importance for their fitness for purpose.

The same conclusion was drawn by ranking all defects detected in each sample in terms of SIF. The analysis showed that in 5 samples out of 10 the maximum SIF corresponded to one of the two defects subjected to the largest applied stress. On the contrary, in only two cases the largest SIF was due to one of the 10 largest defects detected.

Considering the limit load, the deterministic assessment was very much in accordance with the Pro-FACE estimate based on the witness sample (WS). Moreover, the scatter of the 10 data

was well described by considering the experimental variability of defect density. Finally, the simplified calculation made considering all the IPs as superficial yielded a conservative assessment.

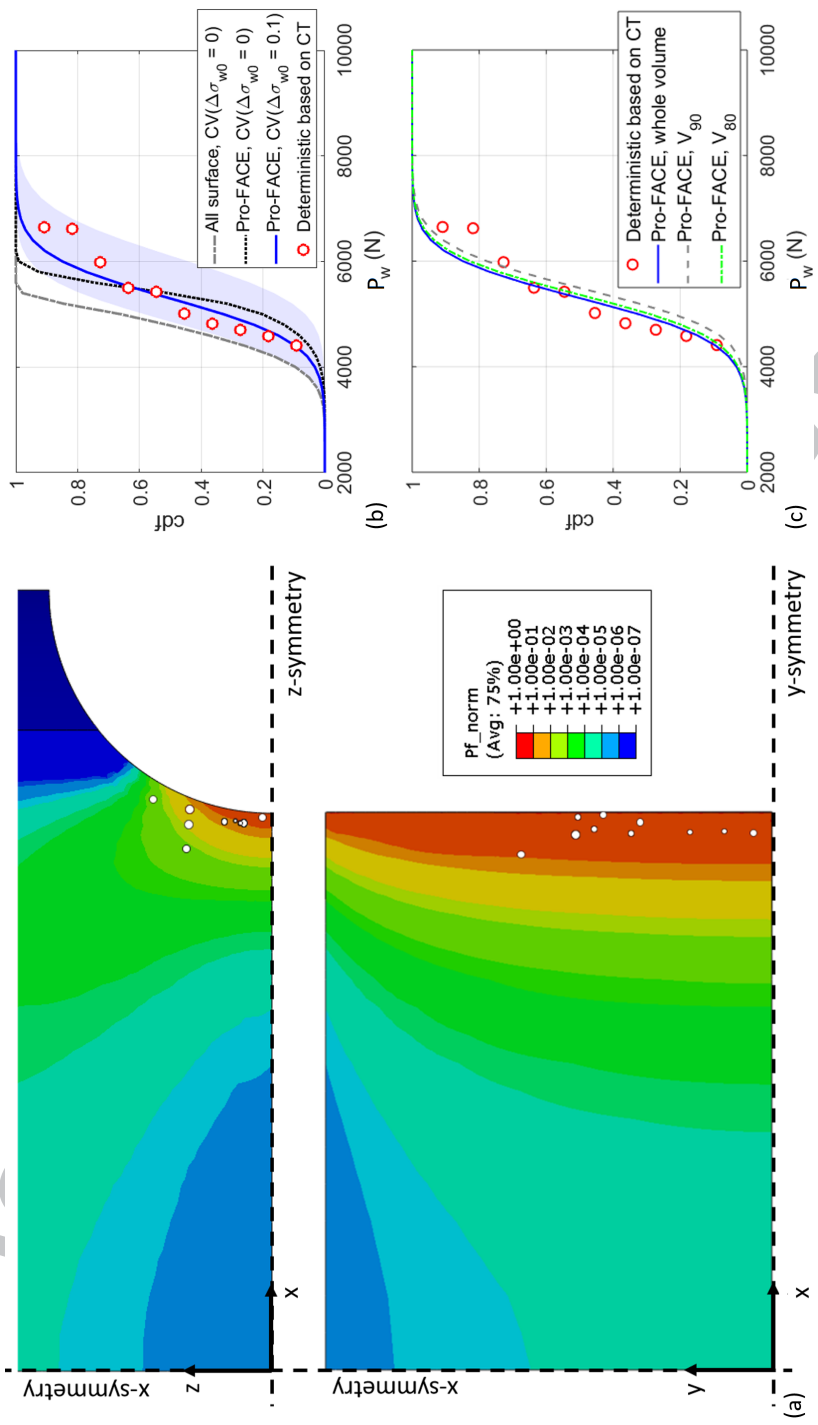

Figure 11: Deterministic and probabilistic assessment of the fatigue limit: (a) location and size of the most critical defect for the samples investigated and probabilistic map of the normalised P_f in the notch region; (b) cdf of the force to be applied to load the batch at the fatigue limit under various assumptions and (c) effect of considering only the most loaded volume.

Finite life assessment

The second step necessary for the verification of Pro-FACE is the finite life assessment in the presence of large stress gradients, which is performed according to the analytical life estimation method presented in Sec. 4.2. The probabilistic and deterministic approaches are based on the same assumptions adopted to assess the fatigue limit.

To verify performance of the implicit life estimation method, state-of-the-art FCG simulations were performed using NASGRO 8.2.
The steps necessary to run the simulations are summarised as follows:

- determining the position and size of the initial crack in every sample on the base of the most critical defect estimated by CT scan and SIF ranking (see Fig. 12a);
- selecting the corresponding crack case in NASGRO. As the position of the critical defect was always on the surface close to the centre of the notches, the crack case selected was "semi-elliptical surface crack in a plate, subjected to a user-defined load field" (SC 31);
- defining the initial size of the crack so that its area is equivalent to that of the critical defect. The initial shape was deemed to be semi-circular;
- define the size of the plate based on the cross-section perpendicular to the applied load containing the critical defect;
- defining the local maximum principal stress field by interpolating the FE results on the plane selected (see a scheme in Fig. 12b);
- creating a user-defined material, based on the experimental results obtained for the material;
- defining the failure condition (in this case, the fulfilment of a 2 mm crack depth).

The simulations were performed considering the five defects with largest SIF detected in every sample, for a total of 50 simulations. Tab. 6 compares the two analyses in terms of overall effort required. A FE analysis was needed in both cases.

Simulation	CT	Other actions	# simulations	Exp. time (w/o CT)
Deterministic NASGRO	All parts	SIF ranking + input for simulations	50	∼1 h per sample
Probabilistic Pro-FACE	One WS	None	1	a few min for the whole batch

Table 6: Summary of the effort required to run the deterministic and probabilistic simulations.

The life distributions for the batch of parts are depicted in Fig. 12c. The picture confirms the good concordance between the deterministic and probabilistic estimates for finite-life assessments. Fig. 12d shows that the estimates performed by Pro-FACE considering the particular defect distribution of every sample slightly improves the precision, as it accounts for the anisotropy in different positions of the platform. In fact, the picture shows that short lives are expected for the samples containing more detrimental defect distributions (i.e., samples 1 to 4) by both the deterministic and probabilistic approaches. Similarly, both methods predict longer lives when the material quality improves (e.g., samples 7 to 9). This confirms that a proper assessment of defect distribution and variability in the platform is fundamental for the application of probabilistic life assessment methods, and that a standardisation of the WS position, size and testing methods is required.

5.3. Discussion on conservatism of Pro-FACE

The implicit life assessment method proposed in Sec. 4.2 proved able to provide fairly good performance. In fact, all life estimates performed yielded conservative results, with an error ranging from below 5% (samples 7 and 9) to a maximum safety factor below 3. The simplicity of the analytical fatigue approach is based on the fulfilment of two main assumptions:

- the SIF applied to any defect is correctly defined;
- a homogeneously stressed volume of material is investigated.

To verify the performance of the simple model for SIF calculation described in Sec. 3.1, the SIF of the ten critical defects was calculated with Murakami's model and compared to the values calculated by NASGRO at the beginning of the FCG simulations (which are based on bi-dimensional weight functions and stress fields). To evaluate the most critical condition, the

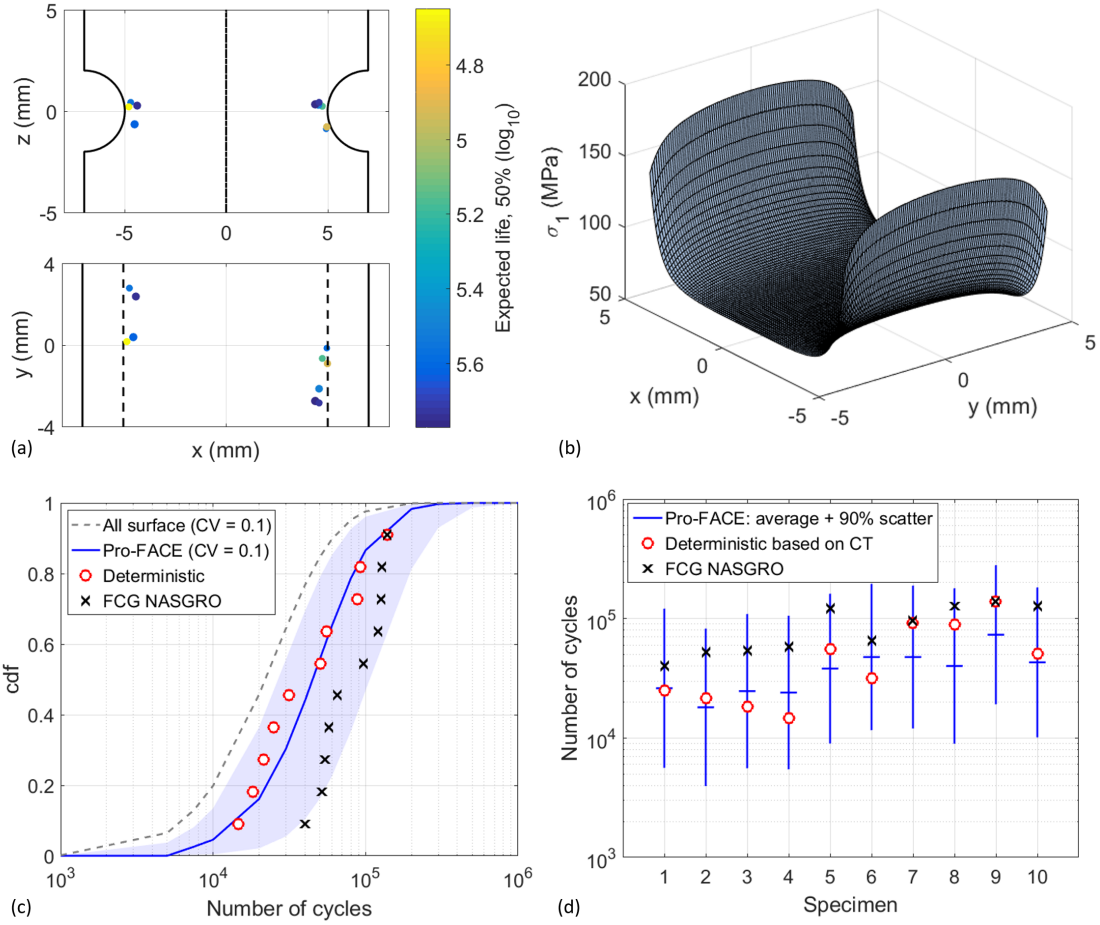

Figure 12: Input for the NASGRO simulations: (a) example position and life expected by Pro-FACE for the ten most critical defects detected in one of the samples; (b) maximum principal stress acting on the plane containing the critical defect (in this example, $z = 0$). Fatigue life estimation by Pro-FACE and NASGRO simulations: (c) cdf for the batch; (d) estimate for every sample.

crack/defect was assumed to be on the surface, in the position of the notched sample subjected to the maximum applied stress.

The findings showed that the simple SIF assessment by Murakami is in accordance with the complex calculation performed by NASGRO, with a difference always below 10% [49]. Note that the calculation based on the weight functions introduces an error too. Considering the huge difference in terms of effort needed for the two analyses, a small approximation can be acceptable for most applications, and it would always be a reasonable compromise during the design phase.

As for the influence of the stress gradient, the small dimension of the defects investigated enables to base the calculations on the punctual stress value of the applied stress computed at the defect centre. This is a perfectly fine assumption for a crack nucleation and early-phase propagation model (i.e., the Kitagawa diagram). However, during the propagation, the crack can extend to regions subjected to different stresses, which can increase or decrease the crack growth rate and therefore the number of cycles to failure. The model presented assumes that the crack remains subjected to the stress initially applied to the defect.

To evaluate the approximation introduced by considering a constant stress along the crack path, the NASGRO simulations were recomputed by setting a constant stress field along the whole crack propagation plane. This assumption was seen to be responsible for most of the conservatism [49]. Some smaller sources of scatter can also be attributed to the intrinsic difference between a fatigue assessment compared to an FCG analysis (e.g., specimen shape, failure condition, intrinsic variability of fatigue and FCG material data).

6. Application to aerospace components

The last step of the analysis is the application of Pro-FACE to a component having a complex geometry, which is usually the case for AM parts. This necessity has pushed to the implementation of the routines inside a FE environment (i.e., Abaqus subroutine) and as an external post-processor. Pro-FACE was used to investigate a bracket designed by RUAG for space application [63] and produced by SLM by process P1 using the AlSi10Mg alloy. All the details about the part, and the input data used for Pro-FACE are reported in [49, 64].

The bracket was proof tested by a series of vibration tests, which were performed by applying both sine and random vibrations along the three principal directions and within a large range of frequencies (0 Hz to 2000 Hz). The target life to withstand the launch was estimated in 1500 cycles, whereas almost no damage is expected above the knee-point of the Wöhler curve ($N_{k,\sigma} = 2 \cdot 10^5$). A safety factor 6 on the life was finally applied in accordance with the fracture control requirements in the presence of detected defects [65, 66]. Fig. 13 depicts the maximum principal stress field determined by FE method when the most detrimental loading condition for the high level sweep test is applied to the part. The part tested survived all the load cases on the shaker with no detectable flaw or stiffness loss. After the tests, the load was increased up to failure to evaluate the most critical region for the structure. The failure happened in the region subjected to the highest stress in Fig. 13, which confirmed the criticality of this loading

condition.

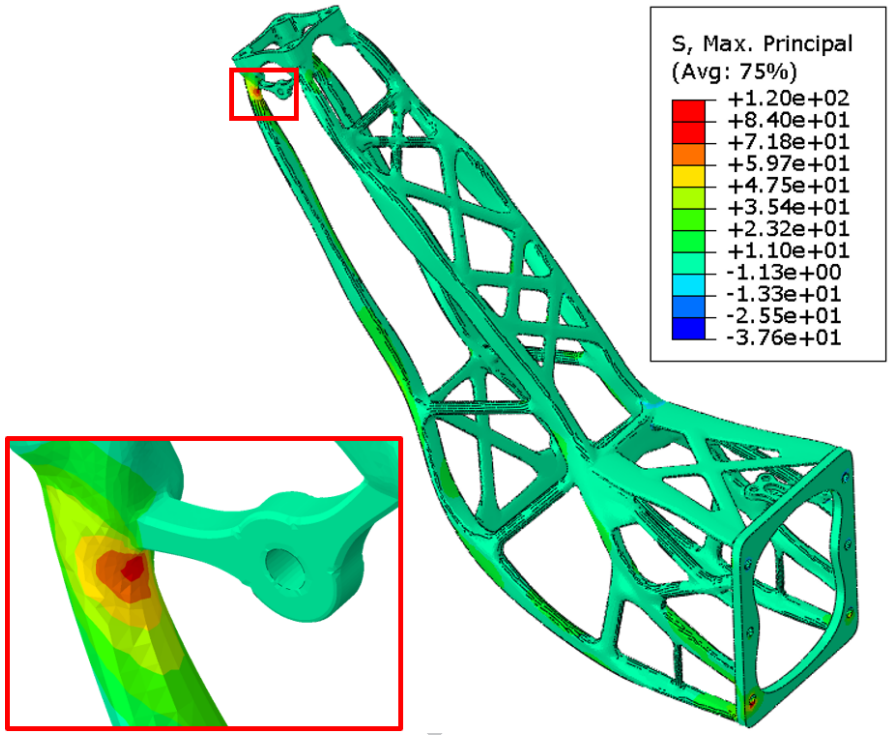

Figure 13: Maximum principal stress determined by FE analysis for the most critical load case.

The results obtained by Pro-FACE about the critical loading condition are depicted in Fig. 14. A first simulation (S1) set the reference result considering all defects in the part as superficial and evaluating as input variable only the defect size distribution. On this basis, the following simulations (S2-S4) respectively added to the foregoing the influence of:

- S2 - refined assessment of defect position, which evaluates the criticality of surface and internal defects as explained in Sec. 3.1;
- S3 - material fatigue strength variability (10% CV based on the experimental results);
- S4 - applied stress (5% CV often used to account for load uncertainties and modelling errors).

As for the variability of the density of defects in the material, this proved to be almost negligible for the present application [64].

Fig. 14a shows that the P_f radically increases when accounting for the strength and stress variabilities. As expected from the full-scale test, the part is very reliable for the target life even

considering the fully-probabilistic assessment (S4). The conservatism introduced by considering all defects as surface (S1) (i.e. the hypothesis of the analytical models available in the literature [29]) proves to be non-negligible in respect of the novel assessment by Pro-FACE (S2). Due to the very low slope of the S-N curve above $N_{k,\sigma}$ cycles, the failure probability above this life tends to flatten. This means that there is a nearly 9% probability that the structure undergoes almost no damage at all, i.e., that none of the defects have enough energy to start propagating.

Another interesting information that can be assessed with Pro-FACE is the performance of the part manufactured adopting different process parameters. As an example, Fig. 14b shows a very large improvement of the reliability from process P1 to P2 and P3, due to the smaller dimensions of the maximum defects [4]. Knowing the material quality achievable according to various process parameters, this analysis could provide important information during the design phase.

Fig. 15 depicts a 3D map of the critical defect size obtained by simulating a life of $N_{k,\sigma}$ cycles. The values refer to a percentile $\mu - 3\,\sigma$ of the distribution of $\sqrt{\text{area}}_{\text{cr}}$.

Finally, it should be borne in mind that the probabilistic assessment is based on the WL assumption that the volumetric defects are randomly spread in the material and on the assumption of mutual independence of microcracks. Considering the Al alloy investigated, this was verified in the WSs. However, this assumption was not acceptable for some regions of the bracket, as clusters of sub-surface pores were detected close to unsupported downfacing surfaces [14]. This issue can be addressed by exploiting the capability of Pro-FACE to distinguish between surface and internal regions, and to differentiate the related distributions. An alternative approach has been presented in [64], which consists in a deterministic evaluation of the most detrimental non-random features detected by NDE.

7. Conclusions

The fatigue properties of AM materials are strictly correlated to the presence of process-dependent inhomogeneities and to the relative scatter of properties with regard to traditional manufacturing processes. This paper has presented a newly developed model for probabilistic fatigue assessment of parts containing manufacturing defects, which was then implemented in the Pro-FACE software. Due to the inevitable presence of process-dependent defects and the capability of Pro-FACE to deal with very complex part shapes and heavy FE models, the tool is naturally suitable to assess the fatigue resistance of metallic AM parts.

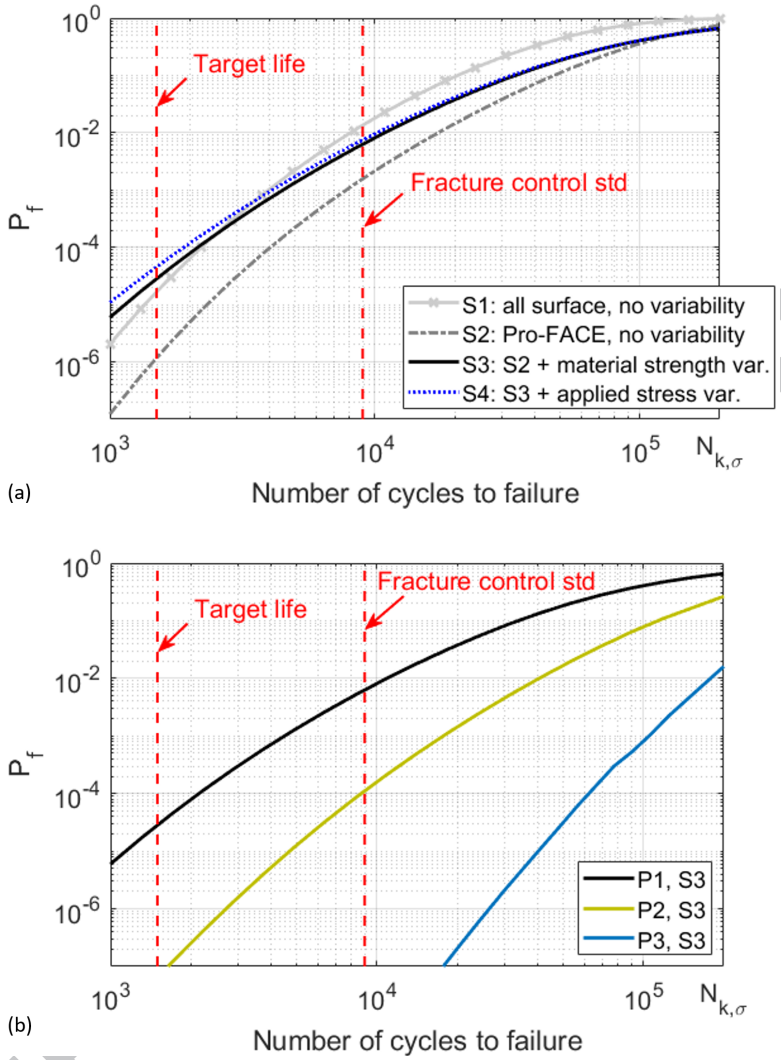

Figure 14: Part P_f for the most detrimental load case as a function of the fatigue life: (a) influence of the main sources of variability for process P1; (b) results expected improving the quality of the manufacturing process from P1 to P3.

Pro-FACE adopts an analytical and mesh-insensitive approach based on the results at the integration points of FE simulations and the Weakest Link model to compute the part failure probability in negligible time compared to the standard FE analysis. A robust evaluation of the fatigue limit is performed based on the Kitagawa diagram of the material, whereas life estimations are computed through a simple assessment based on the Wöhler curve. State-of-the-art FCG simulations have validated the applicability of this approach to notched parts. The life

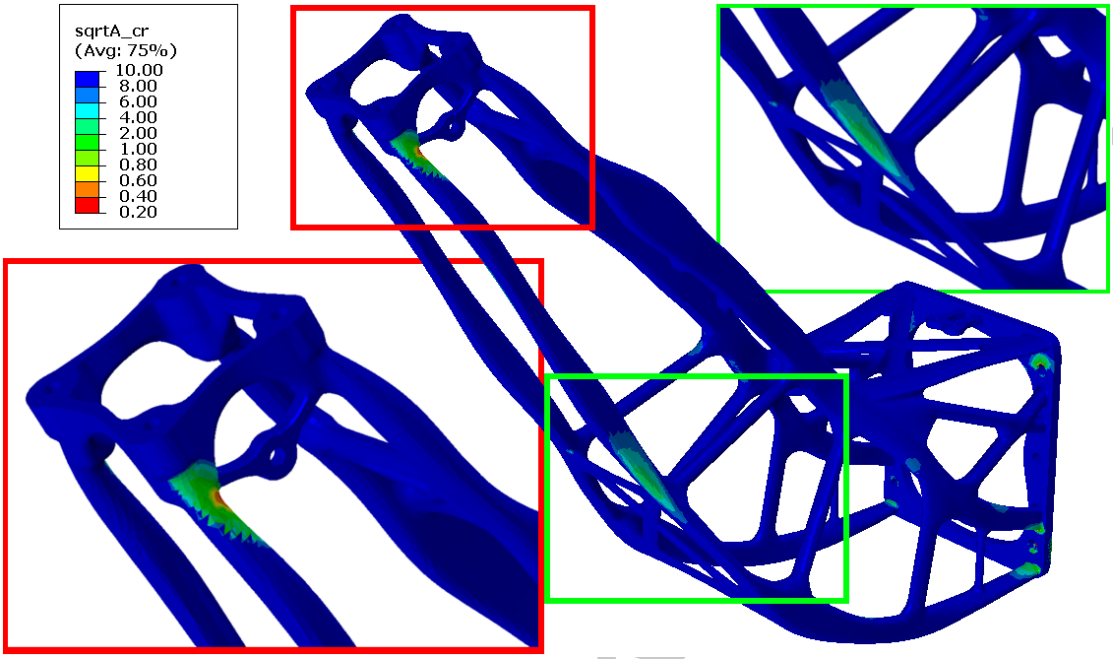

Figure 15: 3D map of critical defect size and location for a percentile $\mu - 3\,\sigma$ (from [64]).

estimations obtained in the presence of steep stress gradients proved to be slightly conservative but required significantly less effort in terms of experimental and simulation efforts.

The implementation to a topologically optimised bracket for space application has demonstrated the capability of Pro-FACE to determine the fatigue resistance and critical regions of complex parts produced by AM, in view of a possible standardised procedure for part assessment. The model has also been used to evaluate the influence of the main sources of variability and has shown the importance of performing a fully-probabilistic assessment to obtain robust results.

Besides the structural assessment, Pro-FACE can be a powerful tool to assess the critical regions during the part concept and design phases, as well as to simulate experimental tests.

Acknowledgements

The validation with notched specimens was supported by the European Space Agency through the NPI Contract No. 4000120615/17 /NL/MH. The authors acknowledge RUAG Space for the permission to publish the results related to the bracket. The validation of the software results for various aerospace parts and metallic alloys is currently ongoing with the support of ESA (AlSi10Mg) and Airbus (Ti-6Al-4V).

References

[1] A. D. Peralta, M. Enright, M. Megahed, J. Gong, M. Roybal, J. Craig, Towards rapid qualification of powder-bed laser additively manufactured parts, Integr. Mater. Manuf. Innov. 5 (1) (2016) 1–23. doi:10.1186/s40192-016-0052-5.

[2] M. Seifi, A. Salem, J. Beuth, O. Harrysson, J. J. Lewandowski, Overview of Materials Qualification Needs for Metal Additive Manufacturing, Jom 68 (3) (2016) 747–764. doi:10.1007/s11837-015-1810-0.

[3] W. E. Frazier, Metal additive manufacturing: a review, Journal of Materials Engineering and Performance 23 (6) (2014) 1917–1928.

[4] S. Romano, A. Brückner-Foit, A. D. Brandão, J. Gumpinger, T. Ghidini, S. Beretta, Fatigue properties of AlSi10Mg obtained by additive manufacturing: Defect-based modelling and prediction of fatigue strength, Engineering Fracture Mechanics 187 (2018) 165–189. doi:10.1016/j.engfracmech.2017.11.002.

[5] U.S. Department of Transportation, FAA Advisory Circular 33.70-1. Guidance Material for Aircraft Engine Life-Limited Parts Requirements (2009).

[6] G. G. Chell, R. C. McClung, D. A. Russell, K. J. Chang, B. Donnelly, Significant A Critical Issues in Proof Testing: A Critical Appraisal, Tech. rep., NASA (1994).

[7] M. Seifi, A. Salem, D. Satko, J. Shaffer, J. J. Lewandowski, Defect distribution and microstructure heterogeneity effects on fracture resistance and fatigue behavior of EBM Ti-6Al-4V, Int. J. Fatigue 94 (2017) 263–287. doi:10.1016/j.ijfatigue.2016.06.001.

[8] George C. Marshall Space Flight Center, Identification Msfc Technical Standard Standard for Additively Manufactured Spaceflight Hardware By Laser Powder Bed Fusion (2017) 93doi:MSFC-STD-3716.

[9] M. Seifi, M. Gorelik, J. Waller, N. Hrabe, N. Shamsaei, S. Daniewicz, J. J. Lewandowski, Progress Towards Metal Additive Manufacturing Standardization to Support Qualification and Certification, Jom 69 (3) (2017) 439–455. doi:10.1007/s11837-017-2265-2.

[10] Y. Murakami, M. Endo, Effect of hardness and crack geometries on $\Delta K_t h$ of small cracks emanating from small defects, in: K. Miller, E. D. L. Rios (Eds.), The Behaviour of Short Fatigue Cracks, MEP, 1986.

[11] Y. Murakami, M. Endo, Effect of defects, inclusions and inhomogeneities on fatigue strength, Int. J. Fatigue 16 (1994) 163–182.

[12] Y. Murakami, Inclusion rating by statistics of extreme values and its application to fatigue strength prediction and quality control of materials., J. Res. Natl. Inst. Stand. Tehcnol. 99 (1994) 345–351.

[13] Y. Murakami, Metal Fatigue: Effects of Small Defects and Nonmetallic Inclusions, Elsevier, Oxford, 2002.

[14] S. Beretta, S. Romano, A comparison of fatigue strength sensitivity to defects for materials manufactured by AM or traditional processes, International Journal of Fatigue 94 (2017) 178–191. doi:10.1016/j.ijfatigue.2016.06.020.

[15] S. Romano, L. Patriarca, S. Foletti, S. Beretta, LCF behaviour and a comprehensive life prediction model for AlSi10Mg obtained by SLM, Int. J. Fatigue 117 (July) (2018) 47–62. doi:10.1016/j.ijfatigue.2018.07.030.

[16] A. Fatemi, R. Molaei, S. Sharifimehr, N. Phan, N. Shamsaei, Multiaxial fatigue behavior of wrought and additive manufactured ti-6al-4v including surface finish effect, International Journal of Fatigue 100 (2017) 347–366.

[17] Y. Yamashita, T. Murakami, R. Mihara, M. Okada, Y. Murakami, Defect analysis and fatigue design basis for ni-based superalloy 718 manufactured by selective laser melting, International Journal of Fatigue 117 (2018) 485–495.

[18] H. Masuo, Y. Tanaka, S. Morokoshi, H. Yagura, T. Uchida, Y. Yamamoto, Y. Murakami, Effects of Defects, Surface Roughness and HIP on Fatigue Strength of Ti-6Al-4V manufactured by Additive Manufacturing, Int. J. Fatiguedoi:10.1016/ j.ijfatigue.2018.07.020.

[19] J. N. D. Ngnekou, Y. Nadot, G. Henaff, J. Nicolai, W. H. Kan, J. M. Cairney, L. Ridosz, Fatigue properties of alsi10mg produced by additive layer manufacturing, International Journal of Fatigue 119 (2019) 160–172.

[20] J. Schijve, Fatigue of Structures and Materials, Kluwer Academic Publishers, Dordrecht, 2001.

[21] H. Bomas, T. Linkewitz, P. Mayr, Application of a weakest-link concepts to the fatigue limit of the bearing steel SAE52100 in a bainitic condition, Fatigue Fract. Engng. Mater. Struct. 22 (1999) 733–741.

[22] A. Brückner-Foit, A. Heger, D. Munz, On the contribution of notches to the failure probability of ceramic components, Journal of the European Ceramic Society 16 (9) (1996) 1027–1034.

[23] W. Weibull, A Statistical Distribution Function of Wide Applicability, Journal of Applied Mechanics (ASME Trans.) 18 (1951) 293–297.

[24] G. Schweiger, K. Heckel, Size effect in randomly loaded specimens, Int. J. Fatigue 8 (4) (1986) 231–234. doi:10.1016/0142-1123(86)90026-5.

[25] G. Härkegård, G. Halleraker, Assessment of methods for prediction of notch and size effects at the fatigue limit based on test data by Böhm and Magin, Int. J. Fatigue 32 (10) (2010) 1701–1709. doi:10.1016/j.ijfatigue.2010.03.011.

[26] A. Diemar, R. Thumser, J. W. Bergmann, Determination of local characteristics for the application of the Weakest-Link Model, Materialwissenschaft und Werkstofftechnikdoi:10.1002/mawe.200400872.

[27] S. Schmitz, T. Seibel, T. Beck, G. Rollmann, R. Krause, H. Gottschalk, A probabilistic model for LCF, Computational Materials Science 79 (2013) 584–590.

[28] S. Beretta, G. Chai, E. Soffiati, A weakest–link analysis for fatigue strength of components containing defects, in: A. Carpinteri (Ed.), Proceedings ICF11, Turin, 2005, p. 975.

[29] A. Wormsen, B. Sjödin, G. Härkegård, A. Fjeldstad, Non-local stress approach for fatigue assessment based on weakest-link theory and statistics of extremes, Fatigue and Fracture of Engineering Materials and Structures 30 (12) (2007) 1214–1227. doi:10.1111/j.1460-2695.2007.01190.x.

[30] A. Wormsen, A. Fjeldstad, G. Härkegård, A post-processor for fatigue crack growth analysis based on a finite element stress field, Computer Methods in Applied Mechanics and Engineering 197 (6-8) (2008) 834–845. doi:10.1016/j.cma.2007.09.012.

[31] A. Fjeldstad, A. Wormsen, G. Härkegård, Simulation of fatigue crack growth in components with random defects, Engineering Fracture Mechanics 75 (5) (2008) 1184–1203.

[32] SwRI, DARWIN.
URL `https://www.swri.org/darwin`

[33] G. Leverant, H. Millwater, R. McClung, M. Enright, A new tool for design and certification of aircraft turbine rotors, J. Engng Gas Turbines Power 126 (2004) 155–159.

[34] R. McClung, , M. Enright, H. Millwater, G. Leverant, S. Hudak, A software Framework for Probabilistic Fatigue Life Assessment of Gas Turbine Engine Rotor, J. ASTM Int. 1 (8).

[35] M. Enright, S. Hudak, R. McClung, Application of Probabilistic Fracture Mechanics to Prognosis of Aircraft Engine Components, AIAA Journal (2006) 311–316.

[36] S. Beretta, S. Foletti, M. Madia, E. Cavalleri, Structural integrity assessment of turbine discs in presence of potential defects: Probabilistic analysis and implementation, Fatigue Fract. Eng. Mater. Struct. 38 (9) (2015) 1042–1055. doi:10.1111/ffe.12325.

[37] E. Gumbel, Statistics of Extremes, Columbia University Press, New York, 1957.

[38] S. Beretta, Y. Murakami, Statistical Analysis of Defects for Fatigue Strength Prediction and Quality Control of Materials, Fatigue Fract. Eng. Mater. Struct. 21 (9) (1998) 1049–1065. doi:doi:10.1046/j.1460-2695.1998.00104.x.

[39] Y. Murakami, S. Beretta, Small Defects and Inhomogeneities in Fatigue Strength: Experiments, Models and Statistical Implications, Extremes 2 (2) (1999) 123–147. doi:10.1023/A:1009976418553.

[40] S. Beretta, C. Anderson, Y. Murakami, Extreme Value Models for the Assessment of Steels Containing Multiple Types of Inclusion, Acta Materialia 5 (54) (2006) 2277–2289.

[41] S. Beretta, Affidabilità delle costruzioni meccaniche: Strumenti e metodi per l'affidabilità di un progetto, Springer Science & Business Media, 2010.

[42] S. Beretta, M. Filippini, P. Luccarelli, A. Motta, G. Pasquero, Assessment of fatigue reliability of power transmission gearing for aerospace propulsion applications, in: ASME Turbo Expo 2013: Turbine Technical Conference and Exposition, no. V07AT28A008, American Society of Mechanical Engineers, 2013.

[43] M. Abramowitz, I. A. Stegun, Integration, in: Handb. Math. Funct. with Formulas, Graphs, Math. Tables, 1983rd Edition, Dover Publications, Washington D.C., 1983, Ch. Chapter 25.

[44] R. C. McClung, Y.-D. Lee, W. Liang, M. P. Enright, S. H. K. Fitch, Automated fatigue crack growth analysis of components, Procedia Eng. 2 (1) (2010) 629–637. doi:http://dx.doi.org/10.1016/j.proeng.2010.03.068.

[45] S. Beretta, Y. Murakami, SIF and threshold for small cracks at small notches under torsion, Fatigue Fract. Eng. Mater. Struct. 23 (2) (2000) 97–104. doi:10.1046/j.1460-2695.2000.00260.x.

[46] S. Romano, A. D. Brandão, J. Gumpinger, M. Gschweitl, S. Beretta, Qualification of AM parts: Extreme value statistics applied to tomographic measurements, Materials & Design 131 (May) (2017) 32–48. doi:10.1016/j.matdes.2017.05.091.

[47] H. Dress, R.-D. Reiss, Tail behavior in wicksell's corpuscle problem, in: Probability Theory and Applications, Springer, 1992, pp. 205–220.

[48] R. Takahashi, M. Sibuya, The maximum size of the planar sections of random spheres and its application to metallurgy, Ann. Inst. Stat. Math. 48 (1) (1996) 127–144. doi:10.1007/BF00049294.

[49] S. Romano, Probabilistic fatigue life assessment of Additive Manufacturing components through computational models, Ph.D. thesis, Politecnico di Milano, Milan, Italy (2018).

[50] S. P. Timoshenko, J. N. Goodier, Theory of elasticity, Vol. 3, McGraw-Hill, New York London, 1970.

[51] D. C. Montgomery, G. C. Runger, Applied Statistics and Probability for Engineers, 6th Edition, John Wiley & Sons, 2014.

[52] K. S. R. Chandran, Duality of fatigue failures of materials caused by Poisson defect statistics of competing failure modes, Nat. Mater. 4 (4) (2005) 303–308. doi:10.1051/nmat1351.

[53] T. Persenot, A. Burr, G. Martin, J.-Y. Buffiere, R. Dendievel, E. Maire, Effect of build orientation on the fatigue properties of as-built Electron Beam Melted Ti-6Al-4V alloy, Int. J. Fatigue 118 (April 2018) (2018) 65–76. doi:10.1016/j.ijfatigue.2018.08.006.

[54] V.-D. Le, E. Pessard, F. Morel, F. Edy, Influence of porosity on the fatigue behaviour of additively fabricated TA6V alloys, in: MATEC Web Conf., Vol. 165, 2018, pp. 1–9. doi:10.1051/matecconf/201816502008.

[55] E. Pessard, D. Bellett, F. Morel, I. Koutiri, A mechanistic approach to the Kitagawa-Takahashi diagram using a multiaxial probabilistic framework, Eng. Fract. Mech. 109 (2013) 89–104. doi:10.1016/j.engfracmech.2013.06.001.

[56] U. Zerbst, M. Vormwald, R. Pippan, H.-P. Gänser, C. Sarrazin-Baudoux, M. Madia, About the fatigue crack propagation threshold of metals as a design criterion–a review, Engineering Fracture Mechanics 153 (2016) 190–243.

[57] S. Beretta, M. Carboni, M. Madia, Modelling of fatigue thresholds for small cracks in a mild steel by "Strip-Yield" model, Engineering Fracture Mechanics 76 (10) (2009) 1548–1561. doi:10.1016/j.engfracmech.2009.04.015.

[58] C. Robert, G. Casella, Monte Carlo statistical methods, Springer Science & Business Media, 2013.

[59] M. Gagnon, A. Tahan, P. Bocher, D. Thibault, Influence of load spectrum assumptions on the expected reliability of hydroelectric turbines: A case study, Structural Safety 50 (2014) 1–8.

[60] Y. Liu, S. Mahadevan, Probabilistic fatigue life prediction using an equivalent initial flaw size distribution, International Journal of Fatigue 31 (3) (2009) 476–487.

[61] R. Kuguel, A relation between theoretical stress concentration factor and fatigue notch factor deduced from the concept of highly stressed volume, in: Proc. ASTM, Vol. 61, 1961, pp. 732–748.

[62] C. M. Sonsino, H. Kaufmann, V. Grubisic, Übertragbarkeit von Werkstoffkennwerten am Beispiel eines betriebsfest auszulegenden geschmiedeten Nutzfahrzeug-Achsschenkels, Konstruktion 47 (7-8) (1995) 222–232.

[63] Moriaux, F., Additive Manufacturing for Space Application, in: Altair technology conference, Paris, 2015, accessed: 2018-04-15.

[64] S. Romano, S. Beretta, S. Miccoli, M. Gschweitl, Probabilistic Framework for Defect Tolerant Fatigue Assessment of AM Parts Applied to a Space Component, Accept. ASTM Sel. Tech. Pap.

[65] ECSS-E-ST-32-01C Rev. 1, Space engineering - Fracture control (2009).

[66] NASA, Fracture Control Requirements For Spaceflight Hardware, NASA Technical standards system (2016) 119.

AppendixA. Integration at Gauss Points

Depending on the applied stress field, on the material resistance (Kitagawa diagram) and on the distribution of the maximum defect in the volume investigated, the function Z of Eq. 15 might be complex. The convergence of the integral of Z with a Gaussian discretisation was evaluated by considering a simple mono-dimensional element subjected to a linear stress gradient (i.e., the stress field obtainable using quadratic FEs). The applied stress considered was varied in the whole range defined by the Kitagawa diagram, as depicted in Fig. A.16a. The function Z, whose trend is shown in Fig. A.16b, was integrated by adopting an increasing number of Gauss points (N_{GP}). The error was defined as the absolute value of the difference between the reconstructed function $Z^*(x)$ (obtained with a polynomial relationship of degree $n = N_{\mathrm{GP}} - 1$) and the correct value $Z(x)$ (see Fig. A.16c)

$$\text{error} = |Z^*(x) - Z(x)|. \tag{A.1}$$

The average error in the element is depicted in Fig. A.16d.

Using linear elements with reduced integration ($N_{\mathrm{GP}} = 1$) causes a very large error in the presence of a stress gradient. The error is substantially reduced by considering two GPs, suggesting the necessity of adopting linear FEs with full integration or quadratic elements with reduced integration. By progressively increasing the number of GPs, the error slightly decreases, but the computational cost increases rapidly. Commonly used quadratic elements with full integration guarantee a small error with a sustainable increase of the computational time. Finally, even more precise results can be obtained by increasing the arbitrary number of GPs, thus going outside the limits of most commercial FE software. Note that, for practical problems with average quality meshes, the stress gradients inside the FEs prove definitely smaller (see Fig. A.17a) and the integral convergence happens much more quickly (Fig. A.17b). In the limit case of elements subjected to a constant stress, the correct solution can be determined using a single GP.

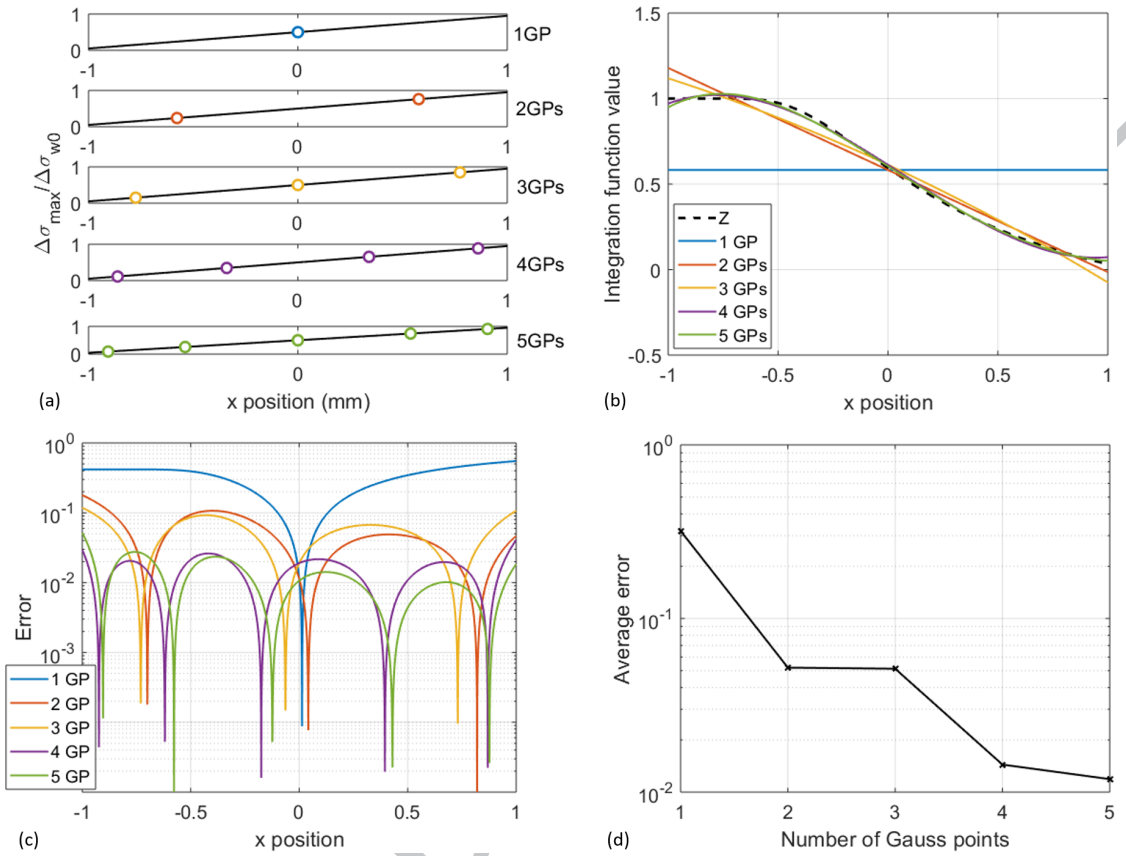

Figure A.16: Precision of the integration varying the number of GPs: (a) applied stress gradient and position of the GPs; (b) integrand function and polynomial approximations using the reconstructed stress field; (c) local percentage error; (d) average error.

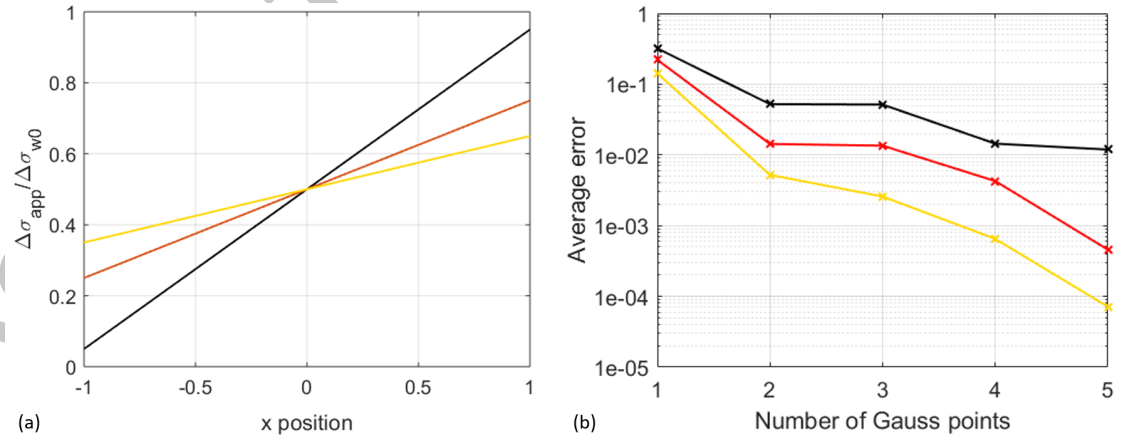

Figure A.17: Precision of the integration varying the stress gradient in the element: (a) applied stress gradient; (b) average error in the element.

- Novel tool for probabilistic fatigue assessment of parts with defects
- Critical defect size and failure probability results validated on notched samples
- The analytic model requires negligible time and computational effort
- New method to evaluate the effect of both surface and internal defects presented
- A fully-probabilistic analysis enables evaluating all major sources of variability

Pro-FACE

Applied stress → Critical defect size

Element volume, Defect distribution → Statistics of extremes → Distribution of maximum defect in each finite element

Critical defect size, Distribution of maximum defect in each finite element → Element failure probability → Weakest link → Component failure probability

Input: Methods: Output: